Theoretical isotope fractionation of cadmium during complexation with organic ligands

Yang Zhao, Yongbing Li, Matthias Wiggenhauser, Geraldine Sarret, Junli Yang, Qi Cheng, Jianming Liu, Yaolin Shi

https://doi.org/10.1016/j.chemgeo.2021.120178
Chemical Geology 571 (2021) 120178

Theoretical Isotope Fractionation of Cadmium during Complexation with Organic Ligands

Yang Zhao [a], Yongbing Li [b,*], Matthias Wiggenhauser [c,d,*], Junli Yang [a],

Géraldine Sarret [c], Qi Cheng [a], Jianming Liu [a, e], Yaolin Shi [b]

[a]*College of Earth and Planetary Sciences, University of Chinese Academy of Sciences, Beijing 100049, China*

[b]*Key Laboratory of Computational Geodynamics, Chinese Academy of Sciences, University of Chinese Academy of Sciences, Beijing 100049, China*

[c]*ISTerre, Univ. Grenoble Alpes, Univ. Savoie Mont Blanc, CNRS, IRD, IFSTTAR, Grenoble, France*

[d]*Institute of Agricultural Sciences, ETH Zurich, Eschikon 33, CH-8315 Lindau, Switzerland*

[e]*Key Laboratory of Mineral Resources, Institute of Geology and Geophysics, Chinese Academy of Sciences, Beijing 100029, China*

*Corresponding authors:
Yongbing Li
No. 19A, Yuquan Road, Shijingshan District, Beijing 100049, PR China.
Tel.: +86 10 88256476.
E-mail address: yongbingli@ucas.ac.cn (Y. Li)

Matthias Wiggenhauser
Institute of Agricultural Sciences, ETH Zurich, Eschikon 33, CH-8315 Lindau, Switzerland
Tel.: +41 52 3549216
E-mail address: matthias.wiggenhauser@usys.ethz.ch (M. W)

Abstract: Cadmium (Cd) isotopes are an important tool to better understand both inorganic and organic geochemistry of Cd, and organic ligands play a key role to control the toxicity and mobility of Cd in living organisms and also in terrestrial and aquatic environments. Knowledge of the equilibrium isotope fractionation of Cd with organic ligands is crucial to further advance Cd isotope source and process tracing in the field of biogeochemistry. In this study, we calculated reduced partition function ratios ($10^3 \ln\beta$) of Cd isotopes in various organic Cd complexes by density functional theory. The calculation results show that the $10^3 \ln\beta$ of $^{114}Cd/^{110}Cd$ for these complexes are decreased in the order of $Cd(Hcit)(H_2cit)^-$ > $Cd(cit)(H_2O)_3^-$ > $CdH(cit)(H_2O)_4$ > CdEDTA > $Cd(his)_2H_2O$ > $Cd(cit)_2^{4-}$ ≈ $Cd(H_2O)_6^{2+}$ > $Cd(H_2O)_4^{2+}$ > $Cd(cys)(H_2O)_3^{2+}$ > $Cd(GS)_2(H_2O)_2^{2-}$ > $Cd(DMPS)(H_2O)_2^-$ > $Cd(DMPS)_2^{4-}$ at 0 ~ 100℃, and heavy Cd isotopes preferably bind to oxygen and nitrogen donor atoms while light Cd isotopes bind to sulfur donor atoms of organic ligands. Thus, the previously observed immobilization of light Cd isotopes in living organisms could be related to Cd detoxification processes with sulfur. The predicted equilibrium isotope fractionation will strengthen Cd isotopes as a process tracing tool in these systems and will improve the understanding of Cd isotope cycling in aquatic and terrestrial systems.

Keywords: Cd isotope; Organic complexes; Equilibrium isotope fractionation; O/N/S donor; Destiny functional theory; Isotope biogeochemistry

1. Introduction

Cadmium (Cd) is a non-essential element for most living organisms (Sigel et al., 2013). It is ubiquitous in terrestrial and aquatic environments where it can occur naturally or through anthropogenic activities (Kabata-Pendias, 2011; Liu et al., 2017). Being very mobile, it is readily taken up by living organisms (Khan et al., 2014; Thévenod et al., 2019), where it can impair the organisms itself (Sigel et al., 2013) and/or it can be further transported along the food chain and accumulated in animals and humans (Fransson et al., 2014; Satarug et al., 2010). Thus, the understanding of processes that control the fate of Cd in the terrestrial and aquatic environments are crucial.

Isotope geochemistry has been increasingly applied in the past years for tracing anthropogenic Cd pollution (Cloquet et al., 2006; Salmanzadeh et al., 2017; Imseng et al., 2018; Yang et al., 2019), tracing the source of ore-forming fluids (Zhu et al., 2016), to advance the understanding of the past and present marine biogeochemical cycling of Cd (Lambelet et al., 2013; Zhang et al., 2018; Sieber et al., 2019), as well as to trace processes that control the Cd homeostasis in unicell organisms (Horner et al., 2013; Moore et al., 2020) and distinct types of plants such as grasses (Wiggenhauser et al., 2016; Imseng et al., 2018; Wiggenhauser et al., 2021; Zhang et al., 2021), cacao (Barraza et al., 2019; Moore et al., 2020), and Cd accumulating plants (Wei et al., 2016; Zhou et al., 2020). Cd has eight stable isotopes which atomic masses range from 106-116, their ratios can vary significantly in the environment

73 (Hoefs, 2015). Cd isotope fractionation in terrestrial and aquatic systems is generated
74 by multiple processes such as sorption to reactive surfaces (Wasylenki et al., 2014),
75 precipitation of Cd into minerals (e.g., calcite, Horner et al., 2011; Guinoiseau et al.,
76 2018; sphalerite, Zhu et al., 2013), membrane transport (Wei et al., 2016), weathering
77 (Zhang et al., 2016; Zhu et al., 2018), binding to inorganic materials (Wasylenki et al.,
78 2014; Yang et al., 2015; Guinoiseau et al., 2018), and complexation with organic
79 ligands as shown for other metals (Morgan et al., 2010; Ryan et al., 2014; Marković et
80 al., 2017). Once isotope fractionation factors are defined for these processes, Cd
81 isotopes can provide novel information about major biogeochemical processes that
82 control the mobility of Cd in complex terrestrial and aquatic systems. For Cd, binding
83 to organic ligands plays a crucial role in detoxifying, sequestrating and separating
84 toxic Cd from essential nutrients in living organisms (Wang and Wang, 2009; Cao et
85 al., 2018; Le Croizier et al., 2019). Recent studies showed that Cd isotopes are
86 strongly fractionated in living organisms which has been attributed to processes such
87 as membrane transport (Moore et al., 2020) and Cd binding to organic ligands
88 (Wiggenhauser et al., 2016, 2018, 2021). For the latter, it was hypothesized that Cd
89 binding to reduced sulfur groups (R-SH, thiols) in the bacteria *E.coli* to detoxify Cd
90 resulted in an enrichment of light isotope in membranes (Horner et al., 2013).
91 Furthermore, cereals strongly retained light Cd isotopes in roots which lead to an
92 enrichment of heavy isotopes in shoots and grains (Wiggenhauser et al., 2016; Imseng
93 et al., 2019; Wiggenhauser et al., 2021; Zhang et al., 2021). The immobilization of
94 light isotopes was ascribed to binding of Cd to thiols to detoxify and sequestrate Cd in

roots and shoot parts and to avoid accumulation of Cd in grains (Wiggenhauser et al., 2016). Together, studies in living organisms proposed that sulfur (S) involved detoxification and immobilization processes of Cd could be a major driver of Cd isotope fractionation. However, no isotope fractionation factor for Cd binding to distinct organic ligands exist yet, which makes it difficult to interpret Cd isotope fractionation in complex biological systems.

During the past few years, calculating isotope fractionation for distinct metal complexes has significantly improved metal isotope process tracing applications in complex biogeochemical systems (Fujii and Albarède, 2012; Moynier et al., 2013; Fujii et al., 2014; Wiederhold, 2015; Albarede et al., 2016; Moynier and Fujii, 2017). For inorganic Cd complexes, theoretical calculations predicted that Cd hydroxides and Cd nitrates are isotopically heavier compared to hydrated Cd while hydrated Cd is heavier than Cd chlorides and hydrosulfide (Yang et al., 2015). Guinoiseau et al. (2018) recently verified these in a Cd sulfide precipitation experiment which revealed that Cd light isotope was enriched in sulfide and that the enrichment of light isotope decreased with increasing chloride concentration in solution. For organic ligands, either experimental or theoretical Cd isotope fractionation data of Cd organic complexes has not been studied. Such Cd isotope fractionation data would be particularly useful to improve Cd isotope process in tracing complex biogeochemical systems where organic ligands play a crucial role on the fate of Cd in the environment. Here, we aimed to strengthen Cd isotope process tracing approaches by applying density functional theory (DFT) to calculate Cd hydrated complexes

117 $Cd(H_2O)_4^{2+}$ and $Cd(H_2O)_6^{2+}$; Cd-citrate complexes $Cd(cit)_2^{4-}$, $Cd(Hcit)(H_2cit)^-$,
118 $CdH(cit)(H_2O)_4$ and $Cd(cit)(H_2O)_3^-$; CdEDTA; Cd-histidine $Cd(his)_2H_2O$; Cd-DMPS
119 complexes $Cd(DMPS)_2^{4-}$ and $Cd(DMPS)(H_2O)_2^-$; Cd-cysteine $Cd(cys)(H_2O)_3^{2+}$; Cd-
120 glutathione complex $Cd(GS)_2(H_2O)_2^{2-}$. The obtained results were discussed regarding
121 its implications for past and future Cd isotope processes tracing approaches.
122
123 **2. Theory and methods**
124
125 *2.1. Cd organic complexes*
126
127 Oxygen (O), nitrogen (N), and sulfur (S) are abundant elements that essential for all
128 living organisms. In organic ligands, they serve as donor atoms to bind metals such as
129 Cd as part of organic complexes such as citrate (cit) (McLean et al., 2013; Panfili et
130 al., 2009; Zorrig et al., 2010), histidine (his) (Wierzbicka et al., 2007; Gunawardana et
131 al., 2010; Hoch et al., 2012; Colaneri et al., 2013), Ethylenediaminetetraacetic acid
132 (EDTA) (Kovács et al., 2010), cysteine (cys) (Leitenmaier et al., 2011; Cao et al.,
133 2014; Smith et al., 2015), glutathione (GSH) (Prévéral et al., 2009; Seth et al., 2011;
134 Wu et al., 2013), and dimercaptopropane sulfonic acid (DMPS) (Zeini Jahromi et al.,
135 2014). These complexes are involved in controlling uptake, transport, and
136 sequestration of Cd in living organisms, whereas EDTA and DMPS are model
137 compounds for strong chelating complexes. EDTA represents chelators with O and N
138 donors such as nicotianamine (Clemens et al., 2013; Marković et al., 2017;

Puschenreiter et al., 2017) and DMPS represents strong chelators with S donors such as phytochelatin (Marentes and Rauser, 2007; Pal et al., 2019).

2.2. Calculations

Equilibrium isotope exchange reaction between two metal complexes can be represented by:

$$AY + BY^* = AY^* + BY \quad (1)$$

where Y denotes one element that is represented by light (Y) and heavy isotopes (Y^*). A and B represent two different ligands. Ligands and isotopes of Y form the chemical complexes AY and BY. The isotope fractionation factor α between the complexes AY and BY is defined as:

$$\alpha_{\text{AY-BY}} = \text{K}_{\text{eq}} = \frac{\beta_{\text{AY}}}{\beta_{\text{BY}}} \quad (2)$$

the isotope fractionation factor is expressed in permill [‰]:

$$10^3 \ln\alpha_{\text{AY-BY}} = 10^3 \ln\beta_{\text{AY}} - 10^3 \ln\beta_{\text{BY}} \quad (3)$$

In these equations, K is the equilibrium constant, which is equal to the α of the isotope exchange reaction of chemical complexes (AY, BY) that exchange the same element (Y). β is the reduced partition function ratio (RPFR). Bigeleisen and Mayer (1947) and Urey (1947) suggested that equilibrium mass-dependent isotope fractionation factors results from the molecular vibrational frequencies. β can be calculated as:

$$\beta_{114-110} = \prod_i \frac{^{114}U_i}{^{110}U_i} \frac{e^{-^{114}U_i/2}}{e^{-^{110}U_i/2}} \frac{1-e^{-^{110}U_i}}{1-e^{-^{114}U_i}} \quad (4)$$

U_i and v_i are defined as:

$$U_i = hv_i / kT \quad (5)$$

Here, h, k, and T refer to the Planck's constant, Boltzmann constant and absolute temperature, respectively. v_i is the harmonic vibrational frequency of the i th vibrational mode in s^{-1}. The number of vibrational modes for non-linear molecules is 3n-6 (n is the number of atoms in the molecule), 3n-5 for linear molecules.

In this study $^{114}Cd/^{110}Cd$ isotope ratios were chosen to study the Cd isotope fractionation of Cd partitioning into different chemical complexes. The $^{114}Cd/^{110}Cd$ is a widely used isotope ratio in experimental (Rehkämper et al., 2011; Horner et al., 2013; Pallavicini et al., 2014; Chrastný et al., 2015; Wei et al., 2016; Li et al., 2018) and theoretical studies (Yang et al., 2015). Gaussian 09 (Dennington et al., 2009; Frisch et al., 2009) was used to calculate the geometries optimization and vibrational frequencies of Cd species using Becke-style 3-parameter (B3) density functional theory with the Lee-Yang-Parr (LYP) correlation functional (Lee et al., 1988; Becke, 1993a, b). In this study, the mixed basis sets were used, for H, C, N, O, and S, the all-electron basis set 6-311+G(d, p) was used (Clark et al., 1983; Francl et al., 1982; Krishnan et al., 1980; McLean and Chandler, 1980; Spitznagel et al., 1987); for Cd, an effective-core potential (ECP) basis set LanL2DZ was chosen (Hay and Wadt, 1985). The "ultrafine" numerical integration grid was used and the molecular geometries were optimized without any forced symmetry for all complexes. The setting of exchange correlation functionals may have effect on the calculated vibrational frequencies, and four exchange correlation functionals B3LYP, BVP86,

183 B3PW91 and PBEPBE were tested. For Cd(Hcit)(H_2cit)$^-$, the mean square errors of
184 the calculated vibrational frequencies of the four exchange correlation functionals are
185 366.90, 874.94, 1084.19 and 7440.05 respectively (Table S1), the calculated
186 frequencies by B3LYP are more consistent with the experimental results and the
187 B3LYP functional was chosen to estimate the isotope fractionation of Cd complexes
188 in this study.
189
190 **3. Results and discussion**
191
192 *3.1. Optimized molecular geometries*
193
194 The optimized geometries of the organic Cd complexes are shown in Fig. 1. For
195 comparison, Table 1 lists the optimized bond lengths calculated by this study, and
196 previously published theoretical and experimental data. Donor atoms, optimized
197 coordinated bond lengths (Å) and mean bond lengths (Å) are shown in Table S3
198 (Supplementary material). The optimized Cd-O distances of $Cd(H_2O)_4^{2+}$ and
199 $Cd(H_2O)_6^{2+}$ (Fig. 1a, b) by using the basis set 6-311+G(d, p) are consistent with those
200 by using the basis set 6-31+G(d, p) (Yang et al., 2015).
201 For Cd-citrate complexes: $Cd(cit)_2^{4-}$, Cd(Hcit)(H_2cit)$^-$, CdH(cit)$(H_2O)_4$ and
202 Cd(cit)$(H_2O)_3^-$, the deprotonated carboxyl groups in Cit^{3-} are always coordinated to
203 the central Cd^{2+} (Bertoli et al., 2015). The d10 electron configuration of Cd^{2+} favors
204 sixfold coordination and forms octahedral geometry (Siddiqui et al., 2011), while in

less bulky ligands, Cd^{2+} tends to form tetrahedral coordination complexes (Ramalho and Figueroa-Villar, 2002; Bertoli et al., 2015). $Cd(cit)_2^{4-}$ (Fig. 1c) and $Cd(Hcit)(H_2cit)^-$ (Fig. 1d) with fourfold coordination complexes, are adducts of two citrate molecules and have several isomers in solution (Bertoli et al., 2015). They differ in their protonation and each of the two citrate molecules provided two carboxylate oxygen atoms to coordinate to Cd^{2+}. The coordinated bond lengths of $Cd(cit)_2^{4-}$ and $Cd(Hcit)(H_2cit)^-$ were 2.21, 2.22 Å and 2.14-2.38 Å respectively. The Cd atoms in $CdH(cit)(H_2O)_4$ (Fig. 1e) and $Cd(cit)(H_2O)_3^-$ (Fig. 1f) were sixfold coordinated, their bond lengths were 2.24-2.40 Å and 2.24-2.43 Å, respectively.

CdEDTA (Fig. 1g) is sixfold coordinated, and EDTA provides two N and four O donor atoms for Cd^{2+}. The stronger binding of Cd^{2+} to N than to O, and the electrostatic attraction induced by the carboxylate result in a high stability for CdEDTA (Kovács et al., 2010; Karak et al., 2016). The calculated Cd-O and Cd-N distances (Cd-O: 2.26, 2.36; Cd-N: 2.48, Table 1b) in this study were close to those calculated by Kovács et al. (2010). Cd-histidine ($Cd(his)_2H_2O$, Fig. 1h) is also sixfold coordinated and contains an imidazole ring, carboxyl and amino groups that provide four N and two O donor atoms for Cd^{2+} (Colaneri et al., 2013). The calculated distances were 2.26 Å for Cd-O 2.41-2.48 Å for Cd-N (Table 1b).

The ligand DMPS contains two thiolate groups and one sulfonate group, and the thiol groups of the DMPS chelate Cd^{2+} in fourfold coordination (Zeini Jahromi et al., 2014, Fig. 1i and 1j). For 1:1 Cd-DMPS complexes, the calculated average distance of Cd to its S donor atoms was 2.48 Å. For 1:2 Cd-DMPS complexes, the average bond

227 distance to four S donor atoms was 2.69 Å. The calculated bond lengths were
228 consistent with the previously published values (Table 1b) (Zeini Jahromi et al.,
229 2014).

230 For $Cd(cys)(H_2O)_3^{2+}$ (Fig. 1k), the thiol group of cysteine tends to bind the metal
231 ion by S donor atoms when cysteine is present in excess (Jalilehvand et al., 2009;
232 Fujii et al., 2014). In our study, Cd was bound to three water molecules and one thiol
233 group of cysteine, the bond length of Cd to its S donor atoms was 2.48 Å, which was
234 slightly shorter than the experimental data of Cd-cysteine 2.52-2.54 Å (Jalilehvand et
235 al., 2009). Glutathione, γ-Glu-Cys-Gly, is a thiol-containing tripeptide, and the
236 ligands of 1:2 Cd-glutathione complexes (Fig. 1l) are GS^{3-} molecules with amide
237 protons, where Cd has a tetrahedral coordination sphere and the complex primarily
238 involves two deprotonated thiol groups from cysteine residues and two water
239 molecules (Delalande et al., 2010). EXAFS spectra of Cd-glutathione complexes
240 suggested Cd was fourfold coordination and S atoms were identified as the binding
241 atoms at 2.54±0.1 Å (Isaure et al., 2015). The calculated Cd-S mean bond distance in
242 this study was in agreement with previous EXAFS result (2.545Å) (Table 1b).

243

244 *3.2. Comparison with experimental vibrational frequencies*

245

246 Only a few experimentally determined vibrational frequencies exist for organic Cd
247 complexes since they are difficult to determine experimentally. Richet et al. (1977)
248 thought the effects of anharmonicity on the isotope fractionation are expected to be

quite small, here only harmonic vibration was considered. Table 2 lists the calculated harmonic vibrational frequencies of the ^{114}w isotopomer and ^{110}w isotopomer of $Cd(Hcit)(H_2cit)^-$ and the experimental data by FTIR (Bertoli et al., 2015). The frequency shifts values $10^3(1 - {}^{114}w/{}^{110}w)$ of Cd isotopes are also listed.

In Table 2, w_1 is the twisting vibration mode of H-C-H with stretching vibration mode of C-O, the experimental vibrational frequencies by Bertoli et al. (2015) was 1027.05 cm^{-1}, the calculated data by this study were 1041.1681 cm^{-1} for ^{114}w isotopomer and 1041.1686 cm^{-1} for ^{110}w isotopomer, the average value of the calculated frequency of the two isotopomers is about 1.375% higher than experimental data. w_2 is the rocking vibration mode of H-C-H with stretching vibration mode of C-C, the experimental data was 1078.98 cm^{-1}, the calculated frequencies were 1079.978 cm^{-1} for Cd heavy isotope and 1079.9783 cm^{-1} for the light one, the average frequency values by this calculation is 0.093% higher than experimental data. w_3 is the twisting vibration mode of H-C-H with stretching vibration mode of C-C, the calculated average data is 1.041% lower than experimental data. w_4 is the scissoring vibration mode of H-C-H, the average data by calculation is close to the experimental data and the calculated average frequency is 0.490% lower than experimental data. w_5 is the rocking vibration mode of H-C-H with stretching vibration mode of C-C and C-O, the average data by calculation is 0.698% higher than experimental data. w_6 is the wagging vibration mode of H-C-H with scissoring vibration mode of O-H, the frequency difference between experiment and the average theory calculation is 0.142%. The w_7 is the symmetrical stretching vibration and the

difference between calculation and experiment is 0.310%. w_8 is the symmetrical stretching vibration mode of COO^-, the difference of calculated data and experimental data is 0.069%. w_9 is asymmetrical stretching vibration of COO^-, the average frequency calculated is 3.187% higher than experimental results. For w_{10}, it is stretching vibration mode and the calculated result is 0.652% lower than experimental data (Table 2). Overall, the calculated frequencies were generally consistent with previously experimental data of $Cd(Hcit)(H_2cit)^-$.

The accuracy of vibrational frequencies can be further propagated in the final $10^3 ln\beta$ values (Schauble et al., 2003, 2004; Schauble et al., 2007). Frequency scaling factors can often be used to correct the calculated vibrational frequencies which are able to reproduce the experimental frequencies. However, the simple harmonic frequency calculated by quantum chemistry methods need to be corrected when it is used to calculate isotope fractionation involving larger molecules (Liu et al., 2010; Fujii et al., 2014). Here frequency scaling factors were not needed in this study.

3.3. Reduced partition function ratios, $10^3 ln(\beta_{114-110})$ for Cd complexes

In nature, mass-independent Cd isotope effects may not be significant and mass dependent effects are the main factor for naturally occurring Cd isotope variations (Rehkämper et al., 2011). Here, only the mass-dependent isotope effects for various Cd species have been studied. The calculated reduced partition function ratios $10^3 ln(\beta_{114-110})$ of the Cd complexes with varying temperatures from 0 °C to 100 °C

calculated in this study are reported in Table 3. ^{114}Cd and ^{110}Cd have the largest mass difference among Cd isotopes (Carignan et al., 2004; Wombacher and Rehkämper, 2004), usually $^{114}Cd/^{110}Cd$ isotope ratios were chosen to study the Cd isotope fractionation of Cd partitioning into different chemical complexes. Mass-dependent isotope fractionation is a function of temperature (T), and can be expressed as below:

$$10^3 \ln(\beta_{114-110}) = A \times \frac{10^6}{T^2} + B \quad (6)$$

Where A, B are the regression parameters, which can be figured out from Table 3. The A, B values of these complexes are listed in Table S2, for comparison their relationship also be figured in Fig. 2. Our calculation shows that the $10^3 \ln\beta$ of $^{114}Cd/^{110}Cd$ for these complexes decreases in the order of $Cd(Hcit)(H_2cit)^-$ > $Cd(cit)(H_2O)_3^-$ > $CdH(cit)(H_2O)_4$ > CdEDTA > $Cd(his)_2H_2O$ > $Cd(cit)_2^{4-}$ ≈ $Cd(H_2O)_6^{2+}$ > $Cd(H_2O)_4^{2+}$ > $Cd(cys)(H_2O)_3^{2+}$ > $Cd(GS)_2(H_2O)_2^{2-}$ > $Cd(DMPS)(H_2O)_2^-$ > $Cd(DMPS)_2^{4-}$ at 0 ~ 100℃.

Previous studies demonstrated that the types of donor atoms (O, N, S) of organic ligands are a main driver for Zn isotope fractionation (Albarède et al., 2011; Fujii and Albarède, 2012; Balter et al., 2013; Moynier et al., 2013; Fujii et al., 2014). Particularly, O donors preferentially bind heavier Zn isotopes than S donors. Cd and Zn are in the same group in the periodic table which means that the two elements have the same number of electrons in their outer valence shell. Thus, the elements share similar chemical properties such as a flexible coordination chemistry, they are non-redox sensitive, and have similar stability constants (John et al., 2017; Maret and Moulis, 2013; Sóvágó and Várnagy, 2013). It is likely that O, N, and S donor atoms

315 may have a similar effect on Cd isotope fractionation as they do for Zn. This
316 hypothesis has been recently partly verified by Yang et al. (2015) who reported an
317 enrichment of heavy Cd isotopes for O and N compared to S donors of inorganic
318 ligands. In addition, studies on Zn isotopes have shown that the number of
319 coordination for the same donor atoms can also determine isotope fractionation (Fujii
320 et al., 2014). For instance, fourfold coordinated Zn-amino acid complexes had larger
321 $10^3\ln(\beta_{114-110})$ values than the sixfold coordinated complexes of the same amino acid.
322 The relationship between the $10^3\ln(\beta_{114-110})$ values and donor atoms type of the Cd
323 complexes at 25℃ is given in Fig. 3 (the types and numbers of donor atoms are given
324 in Table S3). For Cd complexes, S or combinations of S and O donor atoms tended to
325 complex with lighter Cd isotopes. Furthermore, the $10^3\ln(\beta_{114-110})$ disparities induced
326 by S and S/O donor atoms were bigger than those by O and O/N donor atoms. The
327 relationship between $10^3\ln(\beta_{114-110})$ and mean bond lengths of Cd to its donor atoms at
328 25℃ was shown in Fig. 4. Overall, mean coordinated bond lengths of complexes with
329 O donor atoms were shorter than those with S donor atoms, except $Cd(cys)(H_2O)_3^{2+}$.
330 The reason may be that $Cd(cys)(H_2O)_3^{2+}$ has three O donors and one S donor.
331 Among all studied Cd complexes, $Cd(Hcit)(H_2cit)^-$ has the largest $10^3\ln(\beta_{114-110})$
332 values while $Cd(DMPS)_2^{4-}$ has the smallest $10^3\ln(\beta_{114-110})$ values (Fig. 2 and Table 3),
333 their difference can reach 1.18 at 25℃. Cd-citrate complexes can be fourfold
334 coordinated ($Cd(Hcit)(H_2cit)^-$ and $Cd(cit)_2^{4-}$) and sixfold coordinated ($CdH(cit)(H_2O)_4$
335 and $Cd(cit)(H_2O)_3^-$), and their $10^3\ln(\beta_{114-110})$ values can differ up to 0.213 at 25℃
336 which means that the structure difference of these Cd-citrate complexes can result in

Cd isotope fractionation (Fig. 1, 2). In addition, $10^3\ln(\beta_{114-110})$ values of fourfold coordinated $Cd(Hcit)(H_2cit)^-$ were larger than those of sixfold coordinated $CdH(cit)(H_2O)_4$ and $Cd(cit)(H_2O)_3^-$, but those of $Cd(cit)_2^{4-}$ are smaller than those of $CdH(cit)(H_2O)_4$ and $Cd(cit)(H_2O)_3^-$. Thus, for Cd-citrate complexes, the coordination number is only one of the factors that have an effect on Cd isotope fractionation, when estimating Cd isotope fractionation of them, other factors should be considered.

The Cd-cysteine, Cd-GSH, and Cd-DMPS complexes contain S donor atoms. Our calculations revealed that these Cd complexes had lower $10^3\ln(\beta_{114-110})$ values in comparison with hydrated Cd complexes and organic Cd complexes that contained O and N donor atoms (Table 3 and Fig. 3). The lower $10^3\ln(\beta_{114-110})$ values in S containing ligands is in agreement with previous studies that reported $10^3\ln\beta$ values for inorganic Cd (Yang et al., 2015) and organic Zn complexes (Fujii et al., 2014). Among the complexes that contained S and O donor atoms in this study, their $10^3\ln(\beta_{114-110})$ values slightly differed. For instance, $Cd(DMPS)(H_2O)_2^-$ and $Cd(GS)_2(H_2O)_2^{2-}$ were complexed with two S donor atoms from the organic molecules and two O donor atoms from water molecules. The average bond lengths of Cd-S in $Cd(DMPS)(H_2O)_2^-$ (2.48 Å) was shorter than that in $Cd(GS)_2(H_2O)_2^{2-}$ (2.545 Å, Table 1 and S3). The average Cd-O bond lengths in $Cd(DMPS)(H_2O)_2^-$ (2.95 Å) were longer than that of $Cd(GS)_2(H_2O)_2^{2-}$ (2.415 Å). Our data suggests that chelators with S ligands significantly change the bond lengths between Cd and other donor atoms than S which might contribute to the lower $10^3\ln(\beta_{114-110})$ value in the chelating $Cd(DMPS)_2^{4-}$ complex.

As anticipated, the $10^3\ln(\beta_{114-110})$ values of $Cd(DMPS)_2^{4-}$, a Cd chelating complex with four S and no O donor atoms, was smaller compared to $Cd(DMPS)(H_2O)_2^-$ (Table 3 and Fig. 3). This observation agrees with previously published calculations of Zn sulfides where the smallest fractionation occurred in Zn sulfide complexes with four S donor atoms compared to Zn sulfide complexes contained mixtures of S and O donor atoms (Fujii et al., 2011). Together, our data suggests that a large shift towards light isotopes occurs when Cd is complexed to a chelating organic ligand with two or four S donor atoms when compared non-chelating S donor atoms and O/N donor atoms in general.

Experimentally obtained isotope fractionation factors for Zn (Marković et al., 2017) and Cu (Ryan et al., 2014) complexes reported a direct relation between the stability of complexes and the extent and isotope fractionation factors. This relation was also observed in our data, however, the difference of $10^3\ln(\beta_{114-110})$ values between metal chelator CdEDTA and $Cd(his)_2H_2O$ was comparably small (0.027 at 25℃, Fig. 2 and Table 3). Though CdEDTA forms more stable complexes than Cd-histidine complexes (Sóvágó and Várnagy, 2013; Karak et al., 2016), the coordination number was six for both complexes while the CdEDTA had four O and two N donor atoms and $Cd(his)_2H_2O$ had four N and two O donor atoms, and the average bond lengths between the central Cd atom and its donor atoms were very similar: CdEDTA 2.367 Å (Cd-O: 2.26, 2.36 Å; Cd-N: 2.48 Å); $Cd(his)_2H_2O$ 2.378 Å (Cd-O: 2.26 Å; Cd-N: 2.41-2.48 Å, Table S3 and Fig. 4). Hence, the small differences in Cd isotope fractionation between the two complexes might have been demonstrated by the

381 distinct coordination and bond lengths of the two complexes.

382

383 *3.4. Error analysis for Cd isotope fractionation*

384

385 Vacuo and solvation models can cause isotope fractionation factors inaccuracies
386 (Hill and Schauble, 2008; Yang et al., 2015). In ideal vacuum gaseous conditions, the
387 influence of the surrounding environment such as solvents on the solute molecules in
388 the real system is ignored. To overcome this limitation, some solvent models were
389 established to simulate the effects of solvents on solutes. The polarized continuum
390 models (PCMs) are widely used to simulate the aqueous environment (Tomasi et al.,
391 2005; Tsipis, 2014). However, Yang et al. (2015) found that the bond lengths
392 optimized by IEFPCM model are larger than those by vacuo model and the $10^3\ln(\beta_{114-110})$
393 results calculated in the IEFPCM model are smaller than those in vacuo model,
394 and thought that the optimized structures and lnβ values of Cd complexes calculated
395 in vacuo are more consistent with the experimental data. For comparison, the implicit
396 solvation models IEFPCM (the integral-equation-formalism versions of PCM) and
397 CPCM (conductor-like PCM) were used to calculate the optimized molecular
398 structures and $10^3\ln(\beta_{114-110})$ at 25℃ for studied complexes (Table S4 and S5), as well
399 as the model of $Cd(H_2O)_6^{2+}$ with second hydration sphere $Cd(H_2O)_{18}^{2+}$ (Table S6).
400 Our calculation showed that most of the bond lengths optimized in solution by this
401 study were larger than those in vacuum (Table S4). This was agreement with the
402 results of inorganic Cd complexes (Yang et al., 2015). For $10^3\ln(\beta_{114-110})$ values, not

403 only does difference exist between two implicit models and vacuum model but also
404 between two implicit models. By comparing with vacuum model, IEFPCM and
405 CPCM solvation models decrease the $10^3\ln\beta$ of $Cd(H_2O)_4^{2+}$ by 0.346 and 0.221 at 25℃
406 respectively, and increase the $10^3\ln\beta$ of $Cd(H_2O)_6^{2+}$ by 0.139 and 0.166 at 25℃
407 respectively. For $Cd(Hcit)(H_2cit)^-$, $CdH(cit)(H_2O)_4$, $Cd(cit)(H_2O)_3^-$ and $Cd(his)_2H_2O$,
408 IEFPCM and CPCM model decrease the $10^3\ln\beta$ by 0.175-0.580 and 0.206-0.567 and
409 increase the $10^3\ln\beta$ of $Cd(cys)(H_2O)_3^{2+}$ by 0.281 and 0.401 at 25℃ respectively. For
410 $Cd(cit)_2^{4-}$, CdEDTA, $Cd(DMPS)_2^{4-}$, these two models increase the $10^3\ln\beta$ by less than
411 0.1 at 25℃. For $Cd(GS)_2(H_2O)_2^{2-}$, the IEFPCM solvation model decrease the $10^3\ln\beta$
412 by 0.109 and CPCM model increase the $10^3\ln\beta$ by less than 0.1 at 25℃, the implicit
413 solvation models have different effects on Cd isotope fractionation (Table S5). The
414 main reason may be that the simple harmonic vibrational frequencies have been
415 polluted by translation and rotation which make the inaccurate for frequencies data in
416 solvation models (Yang et al., 2015), and the levels of "pollution" may be different for
417 different Cd complexes.

418 Setting the second hydration sphere is able to make the calculated frequencies
419 closer to the experimental values and improve the $10^3\ln\beta$ for Ni and Zn (Fujii et al.,
420 2014), the same phenomenon may occur in Cd hydrate species. Our calculation
421 showed that for $Cd(H_2O)_6^{2+}$, the $10^3\ln\beta$ values for the explicit model as $Cd(H_2O)_{18}^{2+}$
422 is 2.377 and 1.990, 1.923 for explicit model + IEFPCM and explicit model + CPCM
423 at 25℃ respectively. Compared with the vacuum model, the explicit model increases
424 the $10^3\ln\beta$ values and explicit + implicit model decrease them (Table S6). The total

symmetric stretching mode of hexaaqua complexes, ν_1 CdO_6, is shown in Table S6. The calculated ν_1 frequency values of large cluster $Cd(H_2O)_{18}^{2+}$, $Cd(H_2O)_6^{2+}$ + IEFPCM and $Cd(H_2O)_6^{2+}$ + CPCM are closer to previous calculation and experimental data than that of $Cd(H_2O)_6^{2+}$ (Table S6), which means solvation models make the frequency values closer the literature values and the solvent effect on $10^3 ln\beta$ values are needed to be considered.

Frequency is another most frequently mentioned factor that may cause uncertainties or errors of the calculated reduced partition function ratios (Schauble et al., 2003, 2004; Schauble et al., 2007; Méheut et al., 2007, 2009; Weeks et al., 2007; Yang et al., 2015). For lack of experimental vibrational frequency of Cd organic complexes, it is impossible to evaluate the RPFR errors for them, and different vibration frequencies may lead to discrepant uncertainty in $10^3 ln(\beta_{114-110})$ values at 25□ (Vogt et al., 1993; Schauble, 2007; Yang et al., 2015). Based on existing experimental frequency data of $Cd(Hcit)(H_2cit)^-$ and this calculation, the maximum difference between them is 3.187%, and the average deviation is about 0.293%. Based on Schauble (2007, 2011), calculated frequencies may lead to an error of less than 0.6% for $10^3 ln(\beta_{114-110})$ values of $Cd(Hcit)(H_2cit)^-$.

3.5 Implications for Cd process tracing applications in biogeochemistry, supergene geochemistry and environmental science

Metal isotope fractionation can be used to trace processes that control the

447 distribution of an element in terrestrial and aquatic environments. Previous
448 experimental studies hypothesized that the Cd isotope fractionation is strongly linked
449 to Cd speciation to organic ligands with S donor atoms to detoxify and immobilize Cd
450 in living organisms (Horner et al., 2013; Wiggenhauser et al., 2016, 2021; Imseng et
451 al., 2019). Results by this study and Yang et al. (2015) revealed that an enrichment of
452 light isotopes occurs in thiol ligands when compared to hydrated Cd and Cd bound to
453 O/N donor atoms of organic ligands, which will strengthen not only Cd isotopes as a
454 process tracing tool, but also the understanding of Cd isotope cycling in aquatic and
455 terrestrial systems. For example, to reduce inputs of the toxic trace metal Cd into the
456 food chain of humans and animals, processes that control the mobility of Cd in
457 terrestrial and aquatic environments need to be well understood. The results that
458 heavy Cd isotopes preferably bind to oxygen and nitrogen donor atoms while light Cd
459 isotopes bind to sulfur donor atoms of organic ligands compared to hydrated Cd^{2+}
460 provides information on processes on the immobilization of Cd isotopes in living
461 organisms which are related to Cd detoxification processes with sulfur.

462 Furthermore, the strongest Cd isotope fractionation compared to hydrated Cd
463 occurred in chelating S donor ligands, particularly in a chelating S donor ligand in
464 which Cd is exclusively bound to S. Thus, our data confirms the hypothesis that the
465 retention of light isotopes in roots and shoots of grasses (Wiggenhauser et al., 2016,
466 2021; Imseng et al., 2019) and membranes of *E.Coli* (Horner et al., 2013) could be
467 induced by the immobilization of light Cd isotopes through strong Cd binding to
468 chelators with S donor atoms such as phytochelatins (Clemens et al. 2019). This

chelation would retain light Cd isotopes e.g., in the roots of cereals, while other chemical Cd species such as hydrated Cd that are enriched in heavy isotopes can be transported by membrane proteins towards the shoot. The Cd isotope fractionation induced by chelating thiols may have implications on Cd isotope fractionation in other plants than grasses. Cd hyperaccumulator plants can cope with high Cd concentrations and store, unlike cereals, the majority of the Cd taken up from soils in their shoots (Zhou et al. 2020). To cope with the high Cd shoot concentrations, Cd is mostly bound to O donor atoms of e.g., organic acids and to a lesser extent to S donors (Tian et al. 2011; Isaure et al. 2015). Based on our findings, the Cd isotope fractionation in Cd accumulating plants could potentially provide novel insights into the role of Cd binding to different donor atoms on the translocation of Cd within the shoot. Recent studies focused on Cd isotope fractionation in cacao since cacao beans often exceed the threshold values for Cd potentially leading to elevated Cd concentrations in chocolate (Moore et al. 2020; Barraza et al. 2019). Similar to grasses such as wheat, rice, and barley, cacao seems to retain Cd and its light isotopes in the roots (Moore et al. 2020). Our findings suggest that Cd binding to thiols may play also a crucial role to retain Cd in roots of cacao and thereby limit the Cd transport into cacao beans.

Our results further suggest that Cd ligands, especially thiols, may play a key role in Cd isotope fractionation in living organisms, soils, and waters. In this study, the Cd isotope fractionation between hydrated Cd and Cd chelated by S donor atoms was ~ 1‰. The largest Cd isotope fractionation that has been observed between roots and shoots of plants that strongly retain light Cd isotopes in roots was around 0.60 ‰

491 (Wiggenhauser et al. 2016, 2021; Imseng et al. 2018; Moore et al. 2020). The
492 difference between our results and the experimentally determined Cd isotopes
493 fractionation between root and shoots may be caused by additional isotope effects that
494 complement isotope effects at equilibrium. The transfer from root to shoot includes
495 membrane transport (Deng et al. 2019). This transport requires fast binding of Cd to a
496 metal binding site of a membrane protein prior to unidirectional membrane transport
497 (Wang et al., 2014; Zhao et al., 2016). Thus, membrane transport might be at least
498 partly kinetically controlled (Köbberich and Vance, 2017). Kinetically controlled
499 processes favor light isotopes through their faster reaction rates (Wiederhold, 2015)
500 while type of metal binding sites of a membrane transproters (e.g., cysteine, histidine)
501 might play an additional role for isotope fractionation during membrane transport.
502 Together, our results suggest that equilibrium Cd isotope fractionation in plants
503 induced by binding of Cd to organic molecules occur in parallel to kinetic isotope
504 effects.

505 In soils, sediments, and water, organic matter poses an important binding site for
506 Cd and partly controls the mobility of Cd. For instance, soil organic matter derives
507 from decomposed biomass and provides a mixture of O, N, and S donor atoms for Cd
508 in the solid and liquid phase of the soil (Karlsson et al., 2007; Tiberg et al., 2018).
509 Besides processes such as Cd sulfide precipitation and Cd uptake into phytoplankton,
510 soluble organic ligands might significantly control the Cd distribution in water
511 columns and sediments during the oceanic Cd cycle (Guinoiseau et al., 2018). Our
512 data implies that Cd sorption of Cd to organic matter can enrich or deplete the

hydrated Cd pool in heavy and could provide further insights into the role of specific binding sites of organic matter on Cd cycling in the environment.

4. Conclusion

This study provides a first prediction that describes Cd equilibrium isotope fractionation induced by Cd complexation to organic ligands. The $10^3 \ln\beta$ of $^{114}Cd/^{110}Cd$ for these investigated complexes decreased in the order of $Cd(Hcit)(H_2cit)^-$ > $Cd(cit)(H_2O)_3^-$ > $CdH(cit)(H_2O)_4$ > CdEDTA > $Cd(his)_2H_2O$ > $Cd(cit)_2^{4-}$ ≈ $Cd(H_2O)_6^{2+}$ > $Cd(H_2O)_4^{2+}$ > $Cd(cys)(H_2O)_3^{2+}$ > $Cd(GS)_2(H_2O)_2^{2-}$ > $Cd(DMPS)(H_2O)_2^-$ > $Cd(DMPS)_2^{4-}$ at 0 ~ 100℃. The sequence reveals that Cd complexation to organic ligands with O and N donor atoms are enriched in heavy isotopes while to organic ligands with S donor atoms are enriched with light isotopes. These results provide important information to advance Cd isotopes as a process tracing tool in complex biological systems and further improve the understanding of Cd isotope cycling in aquatic and terrestrial systems.

Acknowledgments

This research was supported financially by the National Natural Science Foundation of China (No. 41872160); the Key Project of National Natural Science Foundation of China (No. 41530315); the DREAM project of MOST of China (2016YFC0600401);

535 and the Swiss national research foundation (Early Postdoc.mobility, P2EZP2-
536 178618). We are also grateful for Professor Wang Zhixiang who provided us the
537 chance to conduct this study.

538

539 **Appendices. Supplementary material**

540

541 Table S1: Comparing the experimental vibrational frequencies with calculated results
542 (^{110}w) employed by four different exchange correlation functionals for
543 $Cd(Hcit)(H_2cit)^-$. Table S2: The fitting factors A, B for $10^3\ln(\beta_{114-110})=A\times10^6/T^2+B$ (T
544 is K). Table S3: The donor atoms, coordinated bond lengths (Å) and mean bond
545 lengths (Å) for Cd complexes. Table S4a: Optimized bond lengths (Å) of the Cd
546 hydration complexes and citrate complexes calculated with solvation models. Table
547 S4b: Optimized bond lengths (Å) of the organic Cd complexes calculated with
548 solvation models. Table S5: The $10^3\ln(\beta_{114-110})$ of Cd complexes calculated in vacuo
549 and solvation models (IEFPCM，CPCM) at 25°C. Table S6: The vibrational
550 frequencies (^{110}w) and $10^3\ln\beta$ values of $Cd(H_2O)_6^{2+}$ and $Cd(H_2O)_{18}^{2+}$.

551

552 **References**

553

554 Albarede, F., Télouk, P., Balter, V., Bondanese, V.P., Albalat, E., Oger, P.,
555 Bonaventura, P., Miossec, P., Fujii, T., 2016. Medical applications of Cu, Zn,
556 and S isotope effects. Metallomics 8, 1056–1070.

557 Albarède, F., Telouk, P., Lamboux, A., Jaouen, K., Balter, V., 2011. Isotopic evidence
558 of unaccounted for Fe and Cu erythropoietic pathways. Metallomics 3, 926–933.
559 Balter, V., Lamboux, A., Zazzo, A., Télouk, P., Leverrier, Y., Marvel, J., Moloney,
560 A.P., Monahan, F.J., Schmidt, O., Albarède, F., 2013. Contrasting Cu, Fe, and
561 Zn isotopic patterns in organs and body fluids of mice and sheep, with emphasis
562 on cellular fractionation. Metallomics 5, 1470–1482.
563 Becke, A.D., 1993a. Density- functional thermochemistry. III. The role of exact
564 exchange. J. Chem. Phys. 98, 5648–5652.
565 Becke, A.D., 1993b. A new mixing of Hartree–Fock and local density- functional
566 theories. J. Chem. Phys. 98, 1372–1377.
567 Bertoli, A.C., Carvalho, R., Freitas, M.P., Ramalho, T.C., Mancini, D.T., Oliveira,
568 M.C., de Varennes, A., Dias, A., 2015. Theoretical spectroscopic studies and
569 identification of metal-citrate (Cd and Pb) complexes by ESI-MS in aqueous
570 solution. Spectrochim. Acta Part A Mol. Biomol. Spectrosc. 137, 271–280.
571 Bigalke, M., Weyer, S., Wilcke, W., 2010. Copper isotope fractionation during
572 complexation with insolubilized humic acid. Environ. Sci. Technol. 44, 5496–
573 5502.
574 Bigeleisen, J., Mayer, M.G., 1947. Calculation of equilibrium constants for isotopic
575 exchange reactions. J. Chem. Phys. 15, 261–267.
576 Cao, Z.-Y., Sun, L.-H., Mou, R.-X., Zhou, R., Zhu, Z.-W., Chen, M.-X., 2014. A
577 novel method for the simultaneous analysis of seven biothiols in rice (Oryza
578 sativa L.) using hydrophilic interaction chromatography coupled with

electrospray tandem mass spectrometry. J. Chromatogr. B 976–977.

Cao, Z.-Z., Qin, M.-L., Lin, X.-Y., Zhu, Z.-W., Chen, M.-X., 2018. Sulfur supply reduces cadmium uptake and translocation in rice grains (Oryza sativa L.) by enhancing iron plaque formation, cadmium chelation and vacuolar sequestration. Environ. Pollut. 238, 76–84.

Carignan, J., Cardinal, D., Eisenhauer, A., Galy, A., Rehkämper, M., Wombacher, F., Vigier, N., 2004. A reflection on Mg, Cd, Ca, Li and Si isotopic measurements and related reference materials. Geostand. Geoanalytical Res. 28, 139–148.

Chrastný, V., Čadková, E., Vaněk, A., Teper, L., Cabala, J., Komárek, M., 2015. Cadmium isotope fractionation within the soil profile complicates source identification in relation to Pb–Zn mining and smelting processes. Chem. Geol. 405, 1–9.

Clark, T., Chandrasekhar, J., Spitznagel, G.W., Schleyer, P.V.R., 1983. Efficient diffuse function-augmented basis sets for anion calculations. III. The 3-21+G basis set for first-row elements, Li–F. J. Comput. Chem. 4, 294–301.

Clemens, S., 2019. Metal ligands in micronutrient acquisition and homeostasis. Plant. Cell Environ. 42, 2902–2912.

Clemens, S., Deinlein, U., Ahmadi, H., Höreth, S., Uraguchi, S., 2013. Nicotianamine is a major player in plant Zn homeostasis. BioMetals 26, 623–632.

Cloquet, C., Carignan, J., Libourel, G., Sterckeman, T., Perdrix, E., 2006. Tracing source pollution in soils using cadmium and lead isotopes. Environ. Sci. Technol. 40, 2525–2530.

601 Colaneri, M.J., Vitali, J., Kirschbaum, K., 2013. Electron paramagnetic resonance
602 spectroscopic study of copper hopping in doped bis(l-histidinato)cadmium
603 dihydrate. J. Phys. Chem. A 117, 3414–3427.
604 Deng, F., Yu, M., Martinoia, E., Song, W.-Y., 2019. Ideal Cereals With Lower
605 Arsenic and Cadmium by Accurately Enhancing Vacuolar Sequestration
606 Capacity. Front. Genet. 10, 322.
607 Dennington, R., Keith, T., Millam, J., 2009. GaussView, Version 5.0.8. Semichem
608 Inc.,Shawnee Mission, KS.
609 Delalande, O., Desvaux, H., Godat, E., Valleix, A., Junot, C., Labarre, J., Boulard, Y.,
610 2010. Cadmium – glutathione solution structures provide new insights into
611 heavy metal detoxification. FEBS J. 277, 5086–5096.
612 Francl, M.M., Pietro, W.J., Hehre, W.J., Binkley, J.S., Gordon, M.S., DeFrees, D.J.,
613 Pople, J.A., 1982. Self- consistent molecular orbital methods. XXIII. A
614 polarization- type basis set for second- row elements. J. Chem. Phys. 77, 3654–
615 3665.
616 Fransson, M. N., Barregard, L., Sällsten, G., Akerstrom, M., Johanson, G., 2014.
617 Physiologically-based toxicokinetic model for cadmium using markov-chain
618 monte carlo analysis of concentrations in blood, urine, and kidney cortex from
619 living kidney donors. Toxicol. Sci. 141, 365–376.
620 Frisch, M.J., Trucks, G.W., Schlegel, H.B., Scuseria, G.E., Robb, M.A., Cheeseman,
621 J.R., Scalmani, G., Barone, V., Mennucci, B., Petersson, G.A., Nakatsuji, H.,
622 Caricato, M., Li, X., Hratchian, H.P., Izmaylov, A.F., Bloino, J., Zheng, G.,

623 Sonnenberg, J.L., Hada, M., Ehara, M., Toyota, K., Fukuda, R., Hasegawa, J.,
624 Ishida, M., Nakajima, T., Honda, Y., Kitao, O., Nakai, H., Vreven, T.,
625 Montgomery Jr., J.A., Peralta, J.E., Ogliaro, F., Bearpark, M., Heyd, J.J.,
626 Brothers, E., Kudin, K.N., Staroverov, V.N., Kobayashi, R., Normand, J.,
627 Raghavachari, K., Rendell, A., Burant, J.C., Iyengar, S.S., Tomasi, J., Cossi, M.,
628 Rega, N., Millam, J. M., Klene, M., Knox, J.E., Cross, J.B., Bakken, V., Adamo,
629 C., Jaramillo, J., Gomperts, R., Stratmann, R.E., Yazyev, O., Austin, A.J.,
630 Cammi, R., Pomelli, C., Ochterski, J.W., Martin, R.L., Morokuma, K.,
631 Zakrzewski, V.G., Voth, G.A., Salvador, P., Dannenberg, J.J., Dapprich, S.,
632 Daniels, A.D., Farkas, Ö., Foresman, J.B., Ortiz, J.V., Cioslowski, J., Fox, D.J.,
633 2009. Gaussian 09, Revision A.01. Gaussian, Inc., Wallingford, CT

634 Fujii, T., Albarède, F., 2012. Ab initio calculation of the Zn isotope effect in
635 phosphates, citrates, and malates and applications to plants and soil. PLoS One 7,
636 e30726.

637 Fujii, T., Moynier, F., Blichert-Toft, J., Albarède, F., 2014. Density functional theory
638 estimation of isotope fractionation of Fe, Ni, Cu, and Zn among species relevant
639 to geochemical and biological environments. Geochim. Cosmochim. Acta 140,
640 553–576.

641 Fujii, T., Moynier, F., Pons, M.-L., Albarède, F., 2011. The origin of Zn isotope
642 fractionation in sulfides. Geochim. Cosmochim. Acta 75, 7632–7643.

643 Guinoiseau, D., Galer, S.J.G., Abouchami, W., 2018. Effect of cadmium sulphide
644 precipitation on the partitioning of Cd isotopes: Implications for the oceanic Cd

cycle. Earth Planet. Sci. Lett. 498, 300–308.

Gunawardana, B., Singhal, N., Johnson, A., 2010. Amendments and their combined application for enhanced copper, cadmium, lead uptake byLolium perenne. Plant Soil 329, 283–294.

Hay, P.J., Wadt, W.R., 1985. Ab initio effective core potentials for molecular calculations.Potentials for K to Au including the outer most core orbitals. J. Chem. Phys. 82, 299–310.

Hill, P.S., Schauble, E.A., 2008. Modeling the effects of bond environment on equilibrium iron isotope fractionation in ferric aquo-chloro complexes. Geochim. Cosmochim. Acta 72, 1939–1958.

Hoch, E., Lin, W., Chai, J., Hershfinkel, M., Fu, D., Sekler, I., 2012. Histidine pairing at the metal transport site of mammalian ZnT transporters controls Zn^{2+} over Cd^{2+} selectivity. Proc. Natl. Acad. Sci. 109, 7202–7207.

Hoefs, J., 2015. Isotope fractionation processes of selected elements BT - stable isotope geochemistry, in: Hoefs, J. (Ed.), . Springer International Publishing, Cham, pp. 47–190.

Horner, T.J., Lee, R.B.Y., Henderson, G.M., Rickaby, R.E.M., 2013. Nonspecific uptake and homeostasis drive the oceanic cadmium cycle. Proc. Natl. Acad. Sci. 110, 2500 – 2505.

Horner, T.J., Rickaby, R.E.M., Henderson, G.M., 2011. Isotopic fractionation of cadmium into calcite. Earth Planet. Sci. Lett. 312, 243–253.

Imseng, M., Wiggenhauser, M., Keller, A., Müller, M., Rehkämper, M., Murphy, K.,

667 Kreissig, K., Frossard, E., Wilcke, W., Bigalke, M., 2019. Towards an
668 understanding of the Cd isotope fractionation during transfer from the soil to the
669 cereal grain. Environ. Pollut. 244, 834–844.
670 Imseng, M., Wiggenhauser, M., Keller, A., Müller, M., Rehkämper, M., Murphy, K.,
671 Kreissig, K., Frossard, E., Wilcke, W., Bigalke, M., 2018. Fate of Cd in
672 agricultural soils: a stable isotope approach to anthropogenic impact, soil
673 formation, and soil-plant cycling. Environ. Sci. Technol. 52, 1919–1928.
674 Isaure, M.-P., Huguet, S., Meyer, C.-L., Castillo-Michel, H., Testemale, D., Vantelon,
675 D., Saumitou-Laprade, P., Verbruggen, N., Sarret, G., 2015. Evidence of various
676 mechanisms of Cd sequestration in the hyperaccumulator Arabidopsis halleri, the
677 non-accumulator Arabidopsis lyrata, and their progenies by combined
678 synchrotron-based techniques. J. Exp. Bot. 66, 3201–3214.
679 Jalilehvand, F., Leung, B.O., Mah, V., 2009. Cadmium(II) complex formation with
680 cysteine and penicillamine. Inorg. Chem. 48, 5758–5771.
681 John, S.G., Kunzmann, M., Townsend, E.J., Rosenberg, A.D., 2017. Zinc and
682 cadmium stable isotopes in the geological record: A case study from the post-
683 snowball Earth Nuccaleena cap dolostone. Palaeogeogr. Palaeoclimatol.
684 Palaeoecol. 466, 202–208.
685 Jouvin, D., Louvat, P., Juillot, F., Maréchal, C.N., Benedetti, M.F., 2009. Zinc
686 isotopic fractionation: why organic matters. Environ. Sci. Technol. 43, 5747–
687 5754.
688 Kabata-Pendias, A., 2011. Trace elements in soils and plants, 4. ed. ed. CRC Press,

689 Boca Raton, Fla.
690 Karak, T., Paul, R.K., Das, D.K., Boruah, R.K., 2016. Complexation of DTPA and
691 EDTA with Cd^{2+}: stability constants and thermodynamic parameters at the soil-
692 water interface. Environ. Monit. Assess. 188, 670.
693 Karlsson, T., Elgh-Dalgren, K., Björn, E., Skyllberg, U., 2007. Complexation of
694 cadmium to sulfur and oxygen functional groups in an organic soil. Geochim.
695 Cosmochim. Acta 71, 604–614.
696 Khan, M.A., Castro-Guerrero, N., Mendoza-Cozatl, D.G., 2014. Moving toward a
697 precise nutrition: preferential loading of seeds with essential nutrients over non-
698 essential toxic elements. Front. Plant Sci. 5, 51.
699 Köbberich, M., Vance, D., 2017. Kinetic control on Zn isotope signatures recorded in
700 marine diatoms. Geochim. Cosmochim. Acta 210, 97–113.
701 Kovács, A., Nemcsok, D.S., Kocsis, T., 2010. Bonding interactions in EDTA
702 complexes. J. Mol. Struct. THEOCHEM 950, 93–97.
703 Krishnan, R., Binkley, J.S., Seeger, R., Pople, J.A., 1980. Self- consistent molecular
704 orbital methods. XX. A basis set for correlated wave functions. J. Chem. Phys.
705 72, 650–654.
706 Lambelet, M., Rehkämper, M., van de Flierdt, T., Xue, Z., Kreissig, K., Coles, B.,
707 Porcelli, D., Andersson, P., 2013. Isotopic analysis of Cd in the mixing zone of
708 Siberian rivers with the Arctic Ocean—New constraints on marine Cd cycling
709 and the isotope composition of riverine Cd. Earth Planet. Sci. Lett. 361, 64–73.
710 Larner, F., McLean, C., Halliday, A., Roberts, B., 2019. Copper isotope compositions

711 of superoxide dismutase and metallothionein from post-mortem human frontal
712 cortex. Inorganics 7, 86.
713 Le Croizier, G., Lacroix, C., Artigaud, S., Le Floch, S., Munaron, J.-M., Raffray, J.,
714 Penicaud, V., Rouget, M.-L., Laë, R., Tito De Morais, L., 2019. Metal
715 subcellular partitioning determines excretion pathways and sensitivity to
716 cadmium toxicity in two marine fish species. Chemosphere 217, 754–762.
717 Lee, C., Yang, W., Parr, R.G., 1988. Development of the Colle-Salvetti correlation-
718 energy formula into a functional of the electron density. Phys. Rev. B 37, 785–
719 789.
720 Leitenmaier, B., Witt, A., Witzke, A., Stemke, A., Meyer-Klaucke, W., Kroneck,
721 P.M.H., Küpper, H., 2011. Biochemical and biophysical characterisation yields
722 insights into the mechanism of a Cd/Zn transporting ATPase purified from the
723 hyperaccumulator plant Thlaspi caerulescens. Biochim. Biophys. Acta -
724 Biomembr. 1808, 2591–2599.
725 Li, D., Li, M.-L., Liu, W.-R., Qin, Z.-Z., Liu, S.-A., 2018. Cadmium isotope ratios of
726 standard solutions and geological reference materials measured by MC-ICP-MS.
727 Geostand. Geoanalytical Res. 42, 593–605.
728 Liu, Q., Tossell, J.A., Liu, Y., 2010. On the proper use of the Bigeleisen–Mayer
729 equation and corrections to it in the calculation of isotopic fractionation
730 equilibrium constants. Geochim. Cosmochim. Acta 74, 6965–6983.
731 Liu, Y., Xiao, T., Perkins, R.B., Zhu, J., Zhu, Z., Xiong, Y., Ning, Z., 2017. Geogenic
732 cadmium pollution and potential health risks, with emphasis on black shale. J.

733 Geochemical Explor. 176, 42–49.
734 Marentes, E., Rauser, W.E., 2007. Different proportions of cadmium occur as Cd-
735 binding phytochelatin complexes in plants. Physiol. Plant. 131, 291–301.
736 Maret, W., Moulis, J.-M., 2013. The bioinorganic chemistry of cadmium in the
737 context of its toxicity. Met. Ions Life Sci. 11, 1–29.
738 Marković, T., Manzoor, S., Humphreys-Williams, E., Kirk, G.J.D., Vilar, R., Weiss,
739 D.J., 2017. Experimental determination of zinc isotope fractionation in
740 complexes with the phytosiderophore 2′-deoxymugeneic acid (DMA) and its
741 structural analogues, and implications for plant uptake mechanisms. Environ. Sci.
742 Technol. 51, 98–107.
743 McLean, A.D., Chandler, G.S., 1980. Contracted Gaussian basis sets for molecular
744 calculations. I. Second row atoms, Z=11–18. J. Chem. Phys. 72, 5639–5648.
745 McLean, J.E., Pabst, M.W., Miller, C.D., Dimkpa, C.O., Anderson, A.J., 2013. Effect
746 of complexing ligands on the surface adsorption, internalization, and bioresponse
747 of copper and cadmium in a soil bacterium, Pseudomonas putida. Chemosphere
748 91, 374–382.
749 Méheut, M., Lazzeri, M., Balan, E., Mauri, F., 2007. Equilibrium isotopic
750 fractionation in the kaolinite, quartz, water system: Prediction from first-
751 principles density-functional theory. Geochim. Cosmochim. Acta 71, 3170–3181.
752 Méheut, M., Lazzeri, M., Balan, E., Mauri, F., 2009. Structural control over
753 equilibrium silicon and oxygen isotopic fractionation: A first-principles density-
754 functional theory study. Chem. Geol. 258, 28–37.

Moore, R.E.T., Ullah, I., de Oliveira, V.H., Hammond, S.J., Strekopytov, S., Tibbett, M., Dunwell, J.M., Rehkämper, M., 2020. Cadmium isotope fractionation reveals genetic variation in Cd uptake and translocation by Theobroma cacao and role of natural resistance-associated macrophage protein 5 and heavy metal ATPase-family transporters. Hortic. Res. 7, 71.

Morgan, J.L.L., Wasylenki, L.E., Nuester, J., Anbar, A.D., 2010. Fe Isotope fractionation during equilibration of Fe−organic complexes. Environ. Sci. Technol. 44, 6095–6101.

Moynier, F., Fujii, T., 2017. Theoretical isotopic fractionation of magnesium between chlorophylls. Sci. Rep. 7, 6973.

Moynier, F., Fujii, T., Shaw, A.S., Le Borgne, M., 2013. Heterogeneous distribution of natural zinc isotopes in mice. Metallomics 5, 693–699.

Pal, R., Kaur, R., Rajwar, D., Rai, J., 2019. Induction of non-protein thiols and phytochelatins by cadmium in Eichhornia crassipes. Int. J. Phytoremediation 21, 1–9.

Pallavicini, N., Engström, E., Baxter, D.C., Öhlander, B., Ingri, J., Rodushkin, I., 2014. Cadmium isotope ratio measurements in environmental matrices by MC-ICP-MS. J. Anal. At. Spectrom. 29, 1570–1584.

Panfili, F., Schneider, A., Vives, A., Perrot, F., Hubert, P., Pellerin, S., 2009. Cadmium uptake by durum wheat in presence of citrate. Plant Soil 316, 299–309.

Prévéral, S., Gayet, L., Moldes, C., Hoffmann, J., Mounicou, S., Gruet, A., Reynaud, F., Lobinski, R., Verbavatz, J.-M., Vavasseur, A., Forestier C., 2009. A common

777 highly conserved cadmium detoxification mechanism from bacteria to humans:
778 heavy metal tolerance conferred by the atp-binding cassette (abc) transporter
779 sphmt1 requires glutathione but not metal-chelating phytochelatin peptides. J.
780 Biol. Chem. 284, 4936–4943.
781 Puschenreiter, M., Gruber, B., Wenzel, W.W., Schindlegger, Y., Hann, S., Spangl, B.,
782 Schenkeveld, W.D.C., Kraemer, S.M., Oburger, E., 2017. Phytosiderophore-
783 induced mobilization and uptake of Cd, Cu, Fe, Ni, Pb and Zn by wheat plants
784 grown on metal-enriched soils. Environ. Exp. Bot. 138, 67–76.
785 Ramalho, T.C., Figueroa-Villar, J.D., 2002. Thermodynamic evaluation of complexes
786 of zinc and cadmium that mimetize metallic centers in transcription factors. J.
787 Mol. Struct. THEOCHEM 580, 217–223.
788 Rehkämper, M., Wombacher, F., Horner, T.J., Xue, Z., 2011. Natural and
789 anthropogenic Cd isotope variations. Handbook of Environmental Isotope
790 Geochemistry. Springer, Berlin Heidelberg, pp. 125–154.
791 Richet, P., Bottinga, Y., Javoy, M., 1977. A Review of hydrogen, carbon, nitrogen,
792 oxygen, sulphur, and chlorine stable isotope fractionation among gaseous
793 molecules. Annu. Rev. Earth Planet. Sci. 5, 65–110.
794 Ryan, B.M., Kirby, J.K., Degryse, F., Scheiderich, K., McLaughlin, M.J., 2014.
795 Copper isotope fractionation during equilibration with natural and synthetic
796 ligands. Environ. Sci. Technol. 48, 8620–8626.
797 Salmanzadeh, M., Hartland, A., Stirling, C.H., Balks, M.R., Schipper, L.A., Joshi, C.,
798 George, E., 2017. Isotope tracing of long-term cadmium fluxes in an agricultural

799 soil. Environ. Sci. Technol. 51, 7369–7377.
800 Satarug, S., Garrett, S.H., Sens, M.A., Sens, D.A., 2010. Cadmium, environmental
801 exposure, and health outcomes. Environ. Health Perspect. 118, 182–190.
802 Schauble, E., Rossman, G.R., Taylor, H.P., 2004. Theoretical estimates of equilibrium
803 chromium-isotope fractionations. Chem. Geol. 205, 99–114.
804 Schauble, E.A., 2007. Role of nuclear volume in driving equilibrium stable isotope
805 fractionation of mercury, thallium, and other very heavy elements. Geochim.
806 Cosmochim. Acta 71, 2170–2189.
807 Schauble, E. A., 2011. First-principles estimates of equilibrium magnesium isotope
808 fractionation in silicate, oxide, carbonate and hexaaquamagnesium(2+) crystals.
809 Geochim. Cosmochim. Acta 75(3), 844-869.
810 Schauble, E. A., Rossman, G.R., Taylor, H.P., 2003. Theoretical estimates of
811 equilibrium chlorine-isotope fractionations. Geochim. Cosmochim. Acta 67,
812 3267–3281.
813 Seth, C., Remans, T., Keunen, E., Jozefczak, M., Gielen, H., Opdenakker, K., Weyens,
814 N., Vangronsveld, J., Cuypers, A., 2011. Phytoextraction of toxic metals: A
815 central role for glutathione. Plant. Cell Environ. 35, 334–346.
816 Sieber, M., Conway, T.M., de Souza, G.F., Obata, H., Takano, S., Sohrin, Y., Vance,
817 D., 2019. Physical and biogeochemical controls on the distribution of dissolved
818 cadmium and its isotopes in the Southwest Pacific Ocean. Chem. Geol. 511,
819 494–509.
820 Sigel, A., Sigel, H., Sigel, R.K. (Eds.), 2013. Cadmium: from toxicity to essentiality,

metal ions in life sciences. Springer Netherlands, Dordrecht.

Siddiqui, K.A., Mehrotra, G.K., Narvi, S.S., Butcher, R.J., 2011. Molecular self-assembly of cadmium-triazolate complexes via hydrogen bonding: Synthesis, structures and photoluminescent properties. Inorg. Chem. Commun. 14, 814–817.

Smith, A., Barupala, D., Stemmler, T., Rosenzweig, A., 2015. A new metal binding domain involved in cadmium, cobalt and zinc transport. Nat. Chem. Biol. 11.

Sóvágó, I., Várnagy, K., 2013. Cadmium(II) complexes of amino acids and peptides BT - Cadmium: from toxicity to essentiality, in: Sigel, A., Sigel, H., Sigel, R.K.O. (Eds.), . Springer Netherlands, Dordrecht, pp. 275–302.

Spitznagel, G.W., Clark, T., von Ragué Schleyer, P., Hehre, W.J., 1987. An evaluation of the performance of diffuse function-augmented basis sets for second row elements, Na-Cl. J. Comput. Chem. 8, 1109–1116.

Thévenod, F., Fels, J., Lee, W.-K., Zarbock, R., 2019. Channels, transporters and receptors for cadmium and cadmium complexes in eukaryotic cells: myths and facts. BioMetals 32, 469–489.

Tian, S., Lu, L., Labavitch, J., Yang, X., He, Z., Hu, H., Sarangi, R., Newville, M., Commisso, J., Brown, P., 2011. Cellular Sequestration of Cadmium in the Hyperaccumulator Plant Species Sedum alfredii. Plant Physiol. 157, 1914–1925.

Tiberg, C., Sjöstedt, C., Gustafsson, J.P., 2018. Metal sorption to Spodosol Bs horizons: Organic matter complexes predominate. Chemosphere 196, 556–565.

Tomasi, J., Mennucci, B., Cammi, R., 2005. Quantum mechanical continuum solvation models. Chem. Rev. 105, 2999–3094.

Tsipis, A.C., 2014. DFT flavor of coordination chemistry. Coord. Chem. Rev. 272, 1–29.

Urey, H.C., 1947. The thermodynamic properties of isotopic substances. J. Chem. Soc. 562–581.

Vogt, N., Haaland, A., Martinsen, K.-G., Vogt, J., Grenthe, I., Li, K., MIlanova, R., Nakata, H., Nasiri, A., Tsuda, T., 1993. Molecular parameters of gaseous CdCl2 from electron diffraction and vibrational Spectroscopic data. Acta Chem. Scand. 47, 937–939.

Wang, K. T., Sitsel, O., Meloni, G., Autzen, H., Andersson, M., Klymchuk, T., Nielsen, A., Rees, D., Nissen, P., Gourdon, P., 2014. Structure and mechanism of Zn^{2+}-transporting P-type ATPases. Nature 514.

Wang, M.-J., Wang, W.-X., 2009. Cadmium in three marine phytoplankton: Accumulation, subcellular fate and thiol induction. Aquat. Toxicol. 95, 99–107.

Wasylenki, L.E., Swihart, J.W., Romaniello, S.J., 2014. Cadmium isotope fractionation during adsorption to Mn oxyhydroxide at low and high ionic strength. Geochim. Cosmochim. Acta 140, 212–226.

Weeks, C.L., Anbar, A.D., Wasylenki, L.E., Spiro, T.G., 2007. Density functional theory analysis of molybdenum isotope fractionation. J. Phys. Chem. A 111, 12434–12438.

Wei, R., Guo, Q., Wen, H., Liu, C., Yang, J., Peters, M., Hu, J., Zhu, G., Zhang, H., Tian, L., Han, X., Ma, J., Zhu, C., Wan, Y., 2016. Fractionation of stable cadmium isotopes in the cadmium tolerant ricinus communis and

hyperaccumulator solanum nigrum. Sci. Rep. 6, 24309.

Wiederhold, J.G., 2015. Metal stable isotope signatures as tracers in environmental geochemistry. Environ. Sci. Technol. 49, 2606–2624.

Wierzbicka, M.H., Przedpełska, E., Ruzik, R., Ouerdane, L., Połeć-Pawlak, K., Jarosz, M., Szpunar, J., Szakiel, A., 2007. Comparison of the toxicity and distribution of cadmium and lead in plant cells. Protoplasma 231, 99.

Wiggenhauser, M., Aucour, A.-M., Bureau, S., Campillo, S., Telouk, P., Romani, M., Ma, J.F., Landrot, G., Sarret, G., 2021. Cadmium transfer in contaminated soil-rice systems: Insights from solid-state speciation analysis and stable isotope fractionation. Environ. Pollut. 269, 115934.

Wiggenhauser, M., Bigalke, M., Imseng, M., Müller, M., Keller, A., Murphy, K., Kreissig, K., Rehkämper, M., Wilcke, W., Frossard, E., 2016. Cadmium isotope fractionation in soil–wheat systems. Environ. Sci. Technol. 50, 9223–9231.

Wiggenhauser, M., Bigalke, M., Imseng, M., Keller, A., Archer, C., Wilcke, W.,Frossard, E., 2018. Zinc isotope fractionation during grain filling of wheat and a comparison of zinc and cadmium isotope ratios in identical soil–plant systems. New Phytol. 219, 195–205.

Wombacher, F., Rehkämper, M., 2004. Problems and suggestions concerning the notation of cadmium stable isotope compositions and the use of reference materials. Geostand. Geoanalytical Res. 28, 173–178.

Wu, Z., Zhang, C., Yan, J., Ge, Y., 2013. Separation and quantification of cysteine, glutathione and phytochelatins in rice (Oryza sativa L.) upon cadmium exposure

using reverse phase ultra performance liquid chromatography (RP-UPLC) with fluorescence detection. Anal. Methods 5, 6147–6152.

Yang, J., Li, Y., Liu, S., Tian, H., Chen, C., Liu, J., Shi, Y., 2015. Theoretical calculations of Cd isotope fractionation in hydrothermal fluids. Chem. Geol. 391, 74–82.

Yang, W.-J., Ding, K.-B., Zhang, P., Qiu, H., Cloquet, C., Wen, H.-J., Morel, J.-L., Qiu, R.-L., Tang, Y.-T., 2019. Cadmium stable isotope variation in a mountain area impacted by acid mine drainage. Sci. Total Environ. 646, 696–703.

Zeini Jahromi, E., Gailer, J., Pickering, I.J., George, G.N., 2014. Structural characterization of Cd^{2+} complexes in solution with DMSA and DMPS. J. Inorg. Biochem. 136, 99–106.

Zelano, I.O., Cloquet, C., Fraysse, F., Dong, S., Janot, N., Echevarria, G., Montargès-Pelletier, E., 2018. The influence of organic complexation on Ni isotopic fractionation and Ni recycling in the upper soil layers. Chem. Geol. 483, 47–55.

Zhang, S.-N., Gu, Y., Zhu, Z.-L., Hu, S.-H., Kopittke, P.M., Zhao, F.-J., Wang, P., 2021. Stable isotope fractionation of cadmium in the soil-rice-human continuum. Sci. Total Environ. 761, 143262.

Zhang, Y., Wen, H., Zhu, C., Fan, H., Cloquet, C., 2018. Cadmium isotopic evidence for the evolution of marine primary productivity and the biological extinction event during the Permian-Triassic crisis from the Meishan section, South China. Chem. Geol. 481, 110–118.

Zhang, Y., Wen, H., Zhu, C., Fan, H., Luo, C., Liu, J., Cloquet, C., 2016. Cd isotope

fractionation during simulated and natural weathering. Environ. Pollut. 216, 9–17.

Zhao, C.-M., Campbell, P., Wilkinson, K., 2016. When are metal complexes bioavailable? Environ. Chem. 13, 425–433.

Zhou, J.-W., Li, Z., Liu, M.-S., Yu, H.-M., Wu, L.-H., Huang, F., Luo, Y.-M., Christie, P., 2020. Cadmium Isotopic Fractionation in the Soil–Plant System during Repeated Phytoextraction with a Cadmium Hyperaccumulating Plant Species. Environ. Sci. Technol. 54, 13598–13609.

Zhu, C., Wen, H., Zhang, Y., Fan, H., Fu, S., Xu, J., Qin, T., 2013. Characteristics of Cd isotopic compositions and their genetic significance in the lead–zinc deposits of SW China. Sci. China Earth Sci. 56 (12), 2056–2065.

Zhu, C., Wen, H., Zhang, Y., Fan, H., 2016. Cadmium and sulfur isotopic compositions of the Tianbaoshan Zn–Pb–Cd deposit, Sichuan Province, China. Ore Geol. Rev. 76, 152–162.

Zhu, C., Wen, H., Zhang, Y., Yin, R., Cloquet, C., 2018. Cd isotope fractionation during sulfide mineral weathering in the Fule Zn-Pb-Cd deposit, Yunnan Province, Southwest China. Science of The Total Environment. 616-617, 64-72.

Zorrig, W., Rouached, A., Shahzad, Z., Abdelly, C., Davidian, J.-C., Berthomieu, P., 2010. Identification of three relationships linking cadmium accumulation to cadmium tolerance and zinc and citrate accumulation in lettuce. J. Plant Physiol. 167, 1239–1247.

930 **Figure Captions:**

931

932 **Fig. 1.** Optimized molecular structures for various Cd species. a-b: Cd hydrate; c-f: Cd-citrate, the
933 original source of the structure derives from Bertoli et al. (2015) and Fujii et al. (2012); g:
934 CdEDTA (Kovács et al., 2010); h: Cd-histidine (Colaneri et al., 2013); i-j: Cd-DMPS (Zeini
935 Jahromi et al., 2014); k: Cd-cysteine (Jalilehvand et al., 2009 and Fujii et al., 2014); l: Cd-
936 glutathione (Delalande et al., 2010). Abbreviations are cit (citrate), EDTA
937 (ethylenediaminetetraacetic acid), his (histidine), DMPS (dimercaptopropane sulfonic acid), cys
938 (cysteine), and deprotonated glutathione (GSH) is shown as GS. Symbol keys: H (white), C
939 (grey), N (blue), O (red), S (purple), Cd (yellow).

940 **Fig. 2.** Temperature dependence of $10^3\ln(\beta_{114-110})$ for Cd hydrate, citrate, EDTA, histidine, DMPS,
941 cysteine and glutathione complexes. X-axis shows the function of $10^6/T^2$ (lower shaft) and
942 corresponding temperature (upper shaft, 0-100□), Y-axis shows the $10^3\ln(\beta_{114-110})$ values.

943 **Fig. 3.** Cd ($^{114}Cd/^{110}Cd$) isotopic variations with different donor atoms at 25℃. The complexes
944 with O donor atoms are shown as ⍰; N,O donor complexes as Δ; S,O donor complexes as □; S
945 donor complexes as ○. For O donor complexes, the order of $10^3\ln(\beta_{114-110})$ values at 25℃ from
946 small to large is $Cd(H_2O)_4^{2+}$ < $Cd(H_2O)_6^{2+}$ ≈ $Cd(cit)_2^{4-}$ < $CdH(cit)(H_2O)_4$ < $Cd(cit)(H_2O)_3^-$ <
947 $Cd(Hcit)(H_2cit)^-$; For N,O donor complexes, the order is $Cd(his)_2H_2O$ < CdEDTA; For S,O donor
948 complexes, the order is $Cd(DMPS)(H_2O)_2^-$ < $Cd(GS)_2(H_2O)_2^{2-}$ < $Cd(cys)(H_2O)_3^{2+}$; The S donor
949 complex is $Cd(DMPS)_2^{4-}$.

950 **Fig. 4.** Reduced partition function ratios, $10^3\ln(\beta_{114-110})$ vs. mean bond length (Å) at 25℃. Just as
951 Fig. 3, the complexes with O donor atoms are shown as ⍰, including $Cd(H_2O)_4^{2+}$, $Cd(H_2O)_6^{2+}$,

952 $Cd(cit)_2^{4-}$, $Cd(Hcit)(H_2cit)^-$, $CdH(cit)(H_2O)_4$ and $Cd(cit)(H_2O)_3^-$; N,O donor complexes as Δ,

953 including CdEDTA and $Cd(his)_2H_2O$; S,O donor complexes as □, including $Cd(DMPS)(H_2O)_2^-$,

954 $Cd(cys)(H_2O)_3^{2+}$ and $Cd(GS)_2(H_2O)_2^{2-}$; S donor complex as ○, is $Cd(DMPS)_2^{4-}$.

955

Theoretical Isotope Fractionation of Cadmium during Complexation with Organic Ligands

Yang Zhao [a], Yongbing Li [b,*], Matthias Wiggenhauser [c,d,*], Junli Yang [a], Géraldine Sarret [c], Qi Cheng [a], Jianming Liu [a, e], Yaolin Shi [b]

[a] *College of Earth and Planetary Sciences, University of Chinese Academy of Sciences, Beijing 100049, China*

[b] *Key Laboratory of Computational Geodynamics, Chinese Academy of Sciences, University of Chinese Academy of Sciences, Beijing 100049, China*

[c] *ISTerre, Univ. Grenoble Alpes, Univ. Savoie Mont Blanc, CNRS, IRD, IFSTTAR, Grenoble, France*

[d] *Institute of Agricultural Sciences, ETH Zurich, Eschikon 33, CH-8315 Lindau, Switzerland*

[e] *Key Laboratory of Mineral Resources, Institute of Geology and Geophysics, Chinese Academy of Sciences, Beijing 100029, China*

*Corresponding authors:
Yongbing Li
No. 19A, Yuquan Road, Shijingshan District, Beijing 100049, PR China.
Tel.: +86 10 88256476.
E-mail address: yongbingli@ucas.ac.cn (Y. Li)

Matthias Wiggenhauser
Institute of Agricultural Sciences, ETH Zurich, Eschikon 33, CH-8315 Lindau, Switzerland
Tel.: +41 52 3549216
E-mail address: matthias.wiggenhauser@usys.ethz.ch (M. W)

Abstract: Cadmium **(**Cd) isotopes are an important tool to better understand both inorganic and organic geochemistry of Cd, and organic ligands play a key role to control the toxicity and mobility of Cd in living organisms and also in terrestrial and aquatic environments. Knowledge of the equilibrium isotope fractionation of Cd with organic ligands is crucial to further advance Cd isotope source and process tracing in the field of biogeochemistry. In this study, we calculated reduced partition function ratios ($10^3 ln\beta$) of Cd isotopes in various organic Cd complexes by density functional theory. The calculation results show that the $10^3 ln\beta$ of $^{114}Cd/^{110}Cd$ for these complexes are decreased in the order of $Cd(Hcit)(H_2cit)^-$ > $Cd(cit)(H_2O)_3^-$ > $CdH(cit)(H_2O)_4$ > CdEDTA > $Cd(his)_2H_2O$ > $Cd(cit)_2^{4-}$ ≈ $Cd(H_2O)_6^{2+}$ > $Cd(H_2O)_4^{2+}$ > $Cd(cys)(H_2O)_3^{2+}$ > $Cd(GS)_2(H_2O)_2^{2-}$ > $Cd(DMPS)(H_2O)_2^-$ > $Cd(DMPS)_2^{4-}$ at 0 ~ 100℃, and heavy Cd isotopes preferably bind to oxygen and nitrogen donor atoms while light Cd isotopes bind to sulfur donor atoms of organic ligands. Thus, the previously observed immobilization of light Cd isotopes in living organisms could be related to Cd detoxification processes with sulfur. The predicted equilibrium isotope fractionation will strengthen Cd isotopes as a process tracing tool in these systems and will improve the understanding of Cd isotope cycling in aquatic and terrestrial systems.

Keywords: Cd isotope; Organic complexes; Equilibrium isotope fractionation; O/N/S donor; Destiny functional theory; Isotope biogeochemistry

1. Introduction

Cadmium (Cd) is a non-essential element for most living organisms (Sigel et al., 2013). It is ubiquitous in terrestrial and aquatic environments where it can occur naturally or through anthropogenic activities (Kabata-Pendias, 2011; Liu et al., 2017). Being very mobile, it is readily taken up by living organisms (Khan et al., 2014; Thévenod et al., 2019), where it can impair the organisms itself (Sigel et al., 2013) and/or it can be further transported along the food chain and accumulated in animals and humans (Fransson et al., 2014; Satarug et al., 2010). Thus, the understanding of processes that control the fate of Cd in the terrestrial and aquatic environments are crucial.

Isotope geochemistry has been increasingly applied in the past years for tracing anthropogenic Cd pollution (Cloquet et al., 2006; Salmanzadeh et al., 2017; Imseng et al., 2018; Yang et al., 2019), tracing the source of ore-forming fluids (Zhu et al., 2016), to advance the understanding of the past and present marine biogeochemical cycling of Cd (Lambelet et al., 2013; Zhang et al., 2018; Sieber et al., 2019), as well as to trace processes that control the Cd homeostasis in unicell organisms (Horner et al., 2013; Moore et al., 2020) and distinct types of plants such as grasses (Wiggenhauser et al., 2016; Imseng et al., 2018; Wiggenhauser et al., 2021; Zhang et al., 2021), cacao (Barraza et al., 2019; Moore et al., 2020), and Cd accumulating plants (Wei et al., 2016; Zhou et al., 2020). Cd has eight stable isotopes which atomic masses range from 106-116, their ratios can vary significantly in the environment

(Hoefs, 2015). Cd isotope fractionation in terrestrial and aquatic systems is generated by multiple processes such as sorption to reactive surfaces (Wasylenki et al., 2014), precipitation of Cd into minerals (e.g., calcite, Horner et al., 2011; Guinoiseau et al., 2018; sphalerite, Zhu et al., 2013), membrane transport (Wei et al., 2016), weathering (Zhang et al., 2016; Zhu et al., 2018), binding to inorganic materials (Wasylenki et al., 2014; Yang et al., 2015; Guinoiseau et al., 2018), and complexation with organic ligands as shown for other metals (Morgan et al., 2010; Ryan et al., 2014; Marković et al., 2017). Once isotope fractionation factors are defined for these processes, Cd isotopes can provide novel information about major biogeochemical processes that control the mobility of Cd in complex terrestrial and aquatic systems. For Cd, binding to organic ligands plays a crucial role in detoxifying, sequestrating and separating toxic Cd from essential nutrients in living organisms (Wang and Wang, 2009; Cao et al., 2018; Le Croizier et al., 2019). Recent studies showed that Cd isotopes are strongly fractionated in living organisms which has been attributed to processes such as membrane transport (Moore et al., 2020) and Cd binding to organic ligands (Wiggenhauser et al., 2016, 2018, 2021). For the latter, it was hypothesized that Cd binding to reduced sulfur groups (R-SH, thiols) in the bacteria *E.coli* to detoxify Cd resulted in an enrichment of light isotope in membranes (Horner et al., 2013). Furthermore, cereals strongly retained light Cd isotopes in roots which lead to an enrichment of heavy isotopes in shoots and grains (Wiggenhauser et al., 2016; Imseng et al., 2019; Wiggenhauser et al., 2021; Zhang et al., 2021). The immobilization of light isotopes was ascribed to binding of Cd to thiols to detoxify and sequestrate Cd in

95 roots and shoot parts and to avoid accumulation of Cd in grains (Wiggenhauser et al.,
96 2016). Together, studies in living organisms proposed that sulfur (S) involved
97 detoxification and immobilization processes of Cd could be a major driver of Cd
98 isotope fractionation. However, no isotope fractionation factor for Cd binding to
99 distinct organic ligands exist yet, which makes it difficult to interpret Cd isotope
100 fractionation in complex biological systems.

101 During the past few years, calculating isotope fractionation for distinct metal
102 complexes has significantly improved metal isotope process tracing applications in
103 complex biogeochemical systems (Fujii and Albarède, 2012; Moynier et al., 2013;
104 Fujii et al., 2014; Wiederhold, 2015; Albarede et al., 2016; Moynier and Fujii, 2017).
105 For inorganic Cd complexes, theoretical calculations predicted that Cd hydroxides
106 and Cd nitrates are isotopically heavier compared to hydrated Cd while hydrated Cd is
107 heavier than Cd chlorides and hydrosulfide (Yang et al., 2015). Guinoiseau et al.
108 (2018) recently verified these in a Cd sulfide precipitation experiment which revealed
109 that Cd light isotope was enriched in sulfide and that the enrichment of light isotope
110 decreased with increasing chloride concentration in solution. For organic ligands,
111 either experimental or theoretical Cd isotope fractionation data of Cd organic
112 complexes has not been studied. Such Cd isotope fractionation data would be
113 particularly useful to improve Cd isotope process in tracing complex biogeochemical
114 systems where organic ligands play a crucial role on the fate of Cd in the
115 environment. Here, we aimed to strengthen Cd isotope process tracing approaches by
116 applying density functional theory (DFT) to calculate Cd hydrated complexes

117 $Cd(H_2O)_4^{2+}$ and $Cd(H_2O)_6^{2+}$; Cd-citrate complexes $Cd(cit)_2^{4-}$, $Cd(Hcit)(H_2cit)^-$,
118 $CdH(cit)(H_2O)_4$ and $Cd(cit)(H_2O)_3^-$; CdEDTA; Cd-histidine $Cd(his)_2H_2O$; Cd-DMPS
119 complexes $Cd(DMPS)_2^{4-}$ and $Cd(DMPS)(H_2O)_2^-$; Cd-cysteine $Cd(cys)(H_2O)_3^{2+}$; Cd-
120 glutathione complex $Cd(GS)_2(H_2O)_2^{2-}$. The obtained results were discussed regarding
121 its implications for past and future Cd isotope processes tracing approaches.
122
123 **2. Theory and methods**
124
125 *2.1. Cd organic complexes*
126
127 Oxygen (O), nitrogen (N), and sulfur (S) are abundant elements that essential for all
128 living organisms. In organic ligands, they serve as donor atoms to bind metals such as
129 Cd as part of organic complexes such as citrate (cit) (McLean et al., 2013; Panfili et
130 al., 2009; Zorrig et al., 2010), histidine (his) (Wierzbicka et al., 2007; Gunawardana et
131 al., 2010; Hoch et al., 2012; Colaneri et al., 2013), Ethylenediaminetetraacetic acid
132 (EDTA) (Kovács et al., 2010), cysteine (cys) (Leitenmaier et al., 2011; Cao et al.,
133 2014; Smith et al., 2015), glutathione (GSH) (Prévéral et al., 2009; Seth et al., 2011;
134 Wu et al., 2013), and dimercaptopropane sulfonic acid (DMPS) (Zeini Jahromi et al.,
135 2014). These complexes are involved in controlling uptake, transport, and
136 sequestration of Cd in living organisms, whereas EDTA and DMPS are model
137 compounds for strong chelating complexes. EDTA represents chelators with O and N
138 donors such as nicotianamine (Clemens et al., 2013; Marković et al., 2017;

Puschenreiter et al., 2017) and DMPS represents strong chelators with S donors such as phytochelatin (Marentes and Rauser, 2007; Pal et al., 2019).

2.2. Calculations

Equilibrium isotope exchange reaction between two metal complexes can be represented by:

$$AY + BY^* = AY^* + BY \quad (1)$$

where Y denotes one element that is represented by light (Y) and heavy isotopes (Y^*). A and B represent two different ligands. Ligands and isotopes of Y form the chemical complexes AY and BY. The isotope fractionation factor α between the complexes AY and BY is defined as:

$$\alpha_{\text{AY-BY}} = \text{K}_{\text{eq}} = \frac{\beta_{\text{AY}}}{\beta_{\text{BY}}} \quad (2)$$

the isotope fractionation factor is expressed in permill [‰]:

$$10^3 \ln\alpha_{\text{AY-BY}} = 10^3 \ln\beta_{\text{AY}} - 10^3 \ln\beta_{\text{BY}} \quad (3)$$

In these equations, K is the equilibrium constant, which is equal to the α of the isotope exchange reaction of chemical complexes (AY, BY) that exchange the same element (Y). β is the reduced partition function ratio (RPFR). Bigeleisen and Mayer (1947) and Urey (1947) suggested that equilibrium mass-dependent isotope fractionation factors results from the molecular vibrational frequencies. β can be calculated as:

$$\beta_{114-110} = \prod_i \frac{^{114}U_i}{^{110}U_i} \frac{e^{-^{114}U_i/2}}{e^{-^{110}U_i/2}} \frac{1-e^{-^{110}U_i}}{1-e^{-^{114}U_i}} \quad (4)$$

U_i and v_i are defined as:

$$U_i = h v_i / kT \quad (5)$$

Here, h, k, and T refer to the Planck's constant, Boltzmann constant and absolute temperature, respectively. v_i is the harmonic vibrational frequency of the i th vibrational mode in s^{-1}. The number of vibrational modes for non-linear molecules is 3n-6 (n is the number of atoms in the molecule), 3n-5 for linear molecules.

In this study $^{114}Cd/^{110}Cd$ isotope ratios were chosen to study the Cd isotope fractionation of Cd partitioning into different chemical complexes. The $^{114}Cd/^{110}Cd$ is a widely used isotope ratio in experimental (Rehkämper et al., 2011; Horner et al., 2013; Pallavicini et al., 2014; Chrastný et al., 2015; Wei et al., 2016; Li et al., 2018) and theoretical studies (Yang et al., 2015). Gaussian 09 (Dennington et al., 2009; Frisch et al., 2009) was used to calculate the geometries optimization and vibrational frequencies of Cd species using Becke-style 3-parameter (B3) density functional theory with the Lee-Yang-Parr (LYP) correlation functional (Lee et al., 1988; Becke, 1993a, b). In this study, the mixed basis sets were used, for H, C, N, O, and S, the all-electron basis set 6-311+G(d, p) was used (Clark et al., 1983; Francl et al., 1982; Krishnan et al., 1980; McLean and Chandler, 1980; Spitznagel et al., 1987); for Cd, an effective-core potential (ECP) basis set LanL2DZ was chosen (Hay and Wadt, 1985). The "ultrafine" numerical integration grid was used and the molecular geometries were optimized without any forced symmetry for all complexes. The setting of exchange correlation functionals may have effect on the calculated vibrational frequencies, and four exchange correlation functionals B3LYP, BVP86,

183 B3PW91 and PBEPBE were tested. For $Cd(Hcit)(H_2cit)^-$, the mean square errors of
184 the calculated vibrational frequencies of the four exchange correlation functionals are
185 366.90, 874.94, 1084.19 and 7440.05 respectively (Table S1), the calculated
186 frequencies by B3LYP are more consistent with the experimental results and the
187 B3LYP functional was chosen to estimate the isotope fractionation of Cd complexes
188 in this study.
189
190 **3. Results and discussion**
191
192 *3.1. Optimized molecular geometries*
193
194 The optimized geometries of the organic Cd complexes are shown in Fig. 1. For
195 comparison, Table 1 lists the optimized bond lengths calculated by this study, and
196 previously published theoretical and experimental data. Donor atoms, optimized
197 coordinated bond lengths (Å) and mean bond lengths (Å) are shown in Table S3
198 (Supplementary material). The optimized Cd-O distances of $Cd(H_2O)_4^{2+}$ and
199 $Cd(H_2O)_6^{2+}$ (Fig. 1a, b) by using the basis set 6-311+G(d, p) are consistent with those
200 by using the basis set 6-31+G(d, p) (Yang et al., 2015).
201 For Cd-citrate complexes: $Cd(cit)_2^{4-}$, $Cd(Hcit)(H_2cit)^-$, $CdH(cit)(H_2O)_4$ and
202 $Cd(cit)(H_2O)_3^-$, the deprotonated carboxyl groups in Cit^{3-} are always coordinated to
203 the central Cd^{2+} (Bertoli et al., 2015). The d10 electron configuration of Cd^{2+} favors
204 sixfold coordination and forms octahedral geometry (Siddiqui et al., 2011), while in

less bulky ligands, Cd^{2+} tends to form tetrahedral coordination complexes (Ramalho and Figueroa-Villar, 2002; Bertoli et al., 2015). $Cd(cit)_2^{4-}$ (Fig. 1c) and $Cd(Hcit)(H_2cit)^-$ (Fig. 1d) with fourfold coordination complexes, are adducts of two citrate molecules and have several isomers in solution (Bertoli et al., 2015). They differ in their protonation and each of the two citrate molecules provided two carboxylate oxygen atoms to coordinate to Cd^{2+}. The coordinated bond lengths of $Cd(cit)_2^{4-}$ and $Cd(Hcit)(H_2cit)^-$ were 2.21, 2.22 Å and 2.14-2.38 Å respectively. The Cd atoms in $CdH(cit)(H_2O)_4$ (Fig. 1e) and $Cd(cit)(H_2O)_3^-$ (Fig. 1f) were sixfold coordinated, their bond lengths were 2.24-2.40 Å and 2.24-2.43 Å, respectively.

CdEDTA (Fig. 1g) is sixfold coordinated, and EDTA provides two N and four O donor atoms for Cd^{2+}. The stronger binding of Cd^{2+} to N than to O, and the electrostatic attraction induced by the carboxylate result in a high stability for CdEDTA (Kovács et al., 2010; Karak et al., 2016). The calculated Cd-O and Cd-N distances (Cd-O: 2.26, 2.36; Cd-N: 2.48, Table 1b) in this study were close to those calculated by Kovács et al. (2010). Cd-histidine ($Cd(his)_2H_2O$, Fig. 1h) is also sixfold coordinated and contains an imidazole ring, carboxyl and amino groups that provide four N and two O donor atoms for Cd^{2+} (Colaneri et al., 2013). The calculated distances were 2.26 Å for Cd-O 2.41-2.48 Å for Cd-N (Table 1b).

The ligand DMPS contains two thiolate groups and one sulfonate group, and the thiol groups of the DMPS chelate Cd^{2+} in fourfold coordination (Zeini Jahromi et al., 2014, Fig. 1i and 1j). For 1:1 Cd-DMPS complexes, the calculated average distance of Cd to its S donor atoms was 2.48 Å. For 1:2 Cd-DMPS complexes, the average bond

227 distance to four S donor atoms was 2.69 Å. The calculated bond lengths were
228 consistent with the previously published values (Table 1b) (Zeini Jahromi et al.,
229 2014).

230 For $Cd(cys)(H_2O)_3^{2+}$ (Fig. 1k), the thiol group of cysteine tends to bind the metal
231 ion by S donor atoms when cysteine is present in excess (Jalilehvand et al., 2009;
232 Fujii et al., 2014). In our study, Cd was bound to three water molecules and one thiol
233 group of cysteine, the bond length of Cd to its S donor atoms was 2.48 Å, which was
234 slightly shorter than the experimental data of Cd-cysteine 2.52-2.54 Å (Jalilehvand et
235 al., 2009). Glutathione, γ-Glu-Cys-Gly, is a thiol-containing tripeptide, and the
236 ligands of 1:2 Cd-glutathione complexes (Fig. 1l) are GS^{3-} molecules with amide
237 protons, where Cd has a tetrahedral coordination sphere and the complex primarily
238 involves two deprotonated thiol groups from cysteine residues and two water
239 molecules (Delalande et al., 2010). EXAFS spectra of Cd-glutathione complexes
240 suggested Cd was fourfold coordination and S atoms were identified as the binding
241 atoms at 2.54±0.1 Å (Isaure et al., 2015). The calculated Cd-S mean bond distance in
242 this study was in agreement with previous EXAFS result (2.545Å) (Table 1b).

243

244 *3.2. Comparison with experimental vibrational frequencies*

245

246 Only a few experimentally determined vibrational frequencies exist for organic Cd
247 complexes since they are difficult to determine experimentally. Richet et al. (1977)
248 thought the effects of anharmonicity on the isotope fractionation are expected to be

249 quite small, here only harmonic vibration was considered. Table 2 lists the calculated
250 harmonic vibrational frequencies of the ^{114}w isotopomer and ^{110}w isotopomer of
251 Cd(Hcit)(H_2cit)$^-$ and the experimental data by FTIR (Bertoli et al., 2015). The
252 frequency shifts values $10^3(1 - {}^{114}w/{}^{110}w)$ of Cd isotopes are also listed.

253 In Table 2, w_1 is the twisting vibration mode of H-C-H with stretching vibration
254 mode of C-O, the experimental vibrational frequencies by Bertoli et al. (2015) was
255 1027.05 cm^{-1}, the calculated data by this study were 1041.1681 cm^{-1} for ^{114}w
256 isotopomer and 1041.1686 cm^{-1} for ^{110}w isotopomer, the average value of the
257 calculated frequency of the two isotopomers is about 1.375% higher than
258 experimental data. w_2 is the rocking vibration mode of H-C-H with stretching
259 vibration mode of C-C, the experimental data was 1078.98 cm^{-1}, the calculated
260 frequencies were 1079.978 cm^{-1} for Cd heavy isotope and 1079.9783 cm^{-1} for the
261 light one, the average frequency values by this calculation is 0.093% higher than
262 experimental data. w_3 is the twisting vibration mode of H-C-H with stretching
263 vibration mode of C-C, the calculated average data is 1.041% lower than experimental
264 data. w_4 is the scissoring vibration mode of H-C-H, the average data by calculation is
265 close to the experimental data and the calculated average frequency is 0.490% lower
266 than experimental data. w_5 is the rocking vibration mode of H-C-H with stretching
267 vibration mode of C-C and C-O, the average data by calculation is 0.698% higher
268 than experimental data. w_6 is the wagging vibration mode of H-C-H with scissoring
269 vibration mode of O-H, the frequency difference between experiment and the average
270 theory calculation is 0.142%. The w_7 is the symmetrical stretching vibration and the

difference between calculation and experiment is 0.310%. w_8 is the symmetrical stretching vibration mode of COO^-, the difference of calculated data and experimental data is 0.069%. w_9 is asymmetrical stretching vibration of COO^-, the average frequency calculated is 3.187% higher than experimental results. For w_{10}, it is stretching vibration mode and the calculated result is 0.652% lower than experimental data (Table 2). Overall, the calculated frequencies were generally consistent with previously experimental data of $Cd(Hcit)(H_2cit)^-$.

The accuracy of vibrational frequencies can be further propagated in the final $10^3 ln\beta$ values (Schauble et al., 2003, 2004; Schauble et al., 2007). Frequency scaling factors can often be used to correct the calculated vibrational frequencies which are able to reproduce the experimental frequencies. However, the simple harmonic frequency calculated by quantum chemistry methods need to be corrected when it is used to calculate isotope fractionation involving larger molecules (Liu et al., 2010; Fujii et al., 2014). Here frequency scaling factors were not needed in this study.

3.3. Reduced partition function ratios, $10^3 ln(\beta_{114-110})$ for Cd complexes

In nature, mass-independent Cd isotope effects may not be significant and mass dependent effects are the main factor for naturally occurring Cd isotope variations (Rehkämper et al., 2011). Here, only the mass-dependent isotope effects for various Cd species have been studied. The calculated reduced partition function ratios $10^3 ln(\beta_{114-110})$ of the Cd complexes with varying temperatures from 0 °C to 100 °C

calculated in this study are reported in Table 3. ^{114}Cd and ^{110}Cd have the largest mass difference among Cd isotopes (Carignan et al., 2004; Wombacher and Rehkämper, 2004), usually $^{114}Cd/^{110}Cd$ isotope ratios were chosen to study the Cd isotope fractionation of Cd partitioning into different chemical complexes. Mass-dependent isotope fractionation is a function of temperature (T), and can be expressed as below:

$$10^3 \ln(\beta_{114-110}) = A \times \frac{10^6}{T^2} + B \quad (6)$$

Where A, B are the regression parameters, which can be figured out from Table 3. The A, B values of these complexes are listed in Table S2, for comparison their relationship also be figured in Fig. 2. Our calculation shows that the $10^3 \ln\beta$ of $^{114}Cd/^{110}Cd$ for these complexes decreases in the order of $Cd(Hcit)(H_2cit)^-$ > $Cd(cit)(H_2O)_3^-$ > $CdH(cit)(H_2O)_4$ > CdEDTA > $Cd(his)_2H_2O$ > $Cd(cit)_2^{4-}$ ≈ $Cd(H_2O)_6^{2+}$ > $Cd(H_2O)_4^{2+}$ > $Cd(cys)(H_2O)_3^{2+}$ > $Cd(GS)_2(H_2O)_2^{2-}$ > $Cd(DMPS)(H_2O)_2^-$ > $Cd(DMPS)_2^{4-}$ at 0 ~ 100℃.

Previous studies demonstrated that the types of donor atoms (O, N, S) of organic ligands are a main driver for Zn isotope fractionation (Albarède et al., 2011; Fujii and Albarède, 2012; Balter et al., 2013; Moynier et al., 2013; Fujii et al., 2014). Particularly, O donors preferentially bind heavier Zn isotopes than S donors. Cd and Zn are in the same group in the periodic table which means that the two elements have the same number of electrons in their outer valence shell. Thus, the elements share similar chemical properties such as a flexible coordination chemistry, they are non-redox sensitive, and have similar stability constants (John et al., 2017; Maret and Moulis, 2013; Sóvágó and Várnagy, 2013). It is likely that O, N, and S donor atoms

may have a similar effect on Cd isotope fractionation as they do for Zn. This hypothesis has been recently partly verified by Yang et al. (2015) who reported an enrichment of heavy Cd isotopes for O and N compared to S donors of inorganic ligands. In addition, studies on Zn isotopes have shown that the number of coordination for the same donor atoms can also determine isotope fractionation (Fujii et al., 2014). For instance, fourfold coordinated Zn-amino acid complexes had larger $10^3\ln(\beta_{114-110})$ values than the sixfold coordinated complexes of the same amino acid. The relationship between the $10^3\ln(\beta_{114-110})$ values and donor atoms type of the Cd complexes at 25℃ is given in Fig. 3 (the types and numbers of donor atoms are given in Table S3). For Cd complexes, S or combinations of S and O donor atoms tended to complex with lighter Cd isotopes. Furthermore, the $10^3\ln(\beta_{114-110})$ disparities induced by S and S/O donor atoms were bigger than those by O and O/N donor atoms. The relationship between $10^3\ln(\beta_{114-110})$ and mean bond lengths of Cd to its donor atoms at 25℃ was shown in Fig. 4. Overall, mean coordinated bond lengths of complexes with O donor atoms were shorter than those with S donor atoms, except $Cd(cys)(H_2O)_3^{2+}$. The reason may be that $Cd(cys)(H_2O)_3^{2+}$ has three O donors and one S donor.

Among all studied Cd complexes, $Cd(Hcit)(H_2cit)^-$ has the largest $10^3\ln(\beta_{114-110})$ values while $Cd(DMPS)_2^{4-}$ has the smallest $10^3\ln(\beta_{114-110})$ values (Fig. 2 and Table 3), their difference can reach 1.18 at 25℃. Cd-citrate complexes can be fourfold coordinated ($Cd(Hcit)(H_2cit)^-$ and $Cd(cit)_2^{4-}$) and sixfold coordinated ($CdH(cit)(H_2O)_4$ and $Cd(cit)(H_2O)_3^-$), and their $10^3\ln(\beta_{114-110})$ values can differ up to 0.213 at 25℃ which means that the structure difference of these Cd-citrate complexes can result in

Cd isotope fractionation (Fig. 1, 2). In addition, $10^3\ln(\beta_{114-110})$ values of fourfold coordinated $Cd(Hcit)(H_2cit)^-$ were larger than those of sixfold coordinated $CdH(cit)(H_2O)_4$ and $Cd(cit)(H_2O)_3^-$, but those of $Cd(cit)_2^{4-}$ are smaller than those of $CdH(cit)(H_2O)_4$ and $Cd(cit)(H_2O)_3^-$. Thus, for Cd-citrate complexes, the coordination number is only one of the factors that have an effect on Cd isotope fractionation, when estimating Cd isotope fractionation of them, other factors should be considered.

The Cd-cysteine, Cd-GSH, and Cd-DMPS complexes contain S donor atoms. Our calculations revealed that these Cd complexes had lower $10^3\ln(\beta_{114-110})$ values in comparison with hydrated Cd complexes and organic Cd complexes that contained O and N donor atoms (Table 3 and Fig. 3). The lower $10^3\ln(\beta_{114-110})$ values in S containing ligands is in agreement with previous studies that reported $10^3\ln\beta$ values for inorganic Cd (Yang et al., 2015) and organic Zn complexes (Fujii et al., 2014). Among the complexes that contained S and O donor atoms in this study, their $10^3\ln(\beta_{114-110})$ values slightly differed. For instance, $Cd(DMPS)(H_2O)_2^-$ and $Cd(GS)_2(H_2O)_2^{2-}$ were complexed with two S donor atoms from the organic molecules and two O donor atoms from water molecules. The average bond lengths of Cd-S in $Cd(DMPS)(H_2O)_2^-$ (2.48 Å) was shorter than that in $Cd(GS)_2(H_2O)_2^{2-}$ (2.545 Å, Table 1 and S3). The average Cd-O bond lengths in $Cd(DMPS)(H_2O)_2^-$ (2.95 Å) were longer than that of $Cd(GS)_2(H_2O)_2^{2-}$ (2.415 Å). Our data suggests that chelators with S ligands significantly change the bond lengths between Cd and other donor atoms than S which might contribute to the lower $10^3\ln(\beta_{114-110})$ value in the chelating $Cd(DMPS)_2^{4-}$ complex.

As anticipated, the $10^3\ln(\beta_{114-110})$ values of $Cd(DMPS)_2^{4-}$, a Cd chelating complex with four S and no O donor atoms, was smaller compared to $Cd(DMPS)(H_2O)_2^-$ (Table 3 and Fig. 3). This observation agrees with previously published calculations of Zn sulfides where the smallest fractionation occurred in Zn sulfide complexes with four S donor atoms compared to Zn sulfide complexes contained mixtures of S and O donor atoms (Fujii et al., 2011). Together, our data suggests that a large shift towards light isotopes occurs when Cd is complexed to a chelating organic ligand with two or four S donor atoms when compared non-chelating S donor atoms and O/N donor atoms in general.

Experimentally obtained isotope fractionation factors for Zn (Marković et al., 2017) and Cu (Ryan et al., 2014) complexes reported a direct relation between the stability of complexes and the extent and isotope fractionation factors. This relation was also observed in our data, however, the difference of $10^3\ln(\beta_{114-110})$ values between metal chelator CdEDTA and $Cd(his)_2H_2O$ was comparably small (0.027 at 25℃, Fig. 2 and Table 3). Though CdEDTA forms more stable complexes than Cd-histidine complexes (Sóvágó and Várnagy, 2013; Karak et al., 2016), the coordination number was six for both complexes while the CdEDTA had four O and two N donor atoms and $Cd(his)_2H_2O$ had four N and two O donor atoms, and the average bond lengths between the central Cd atom and its donor atoms were very similar: CdEDTA 2.367 Å (Cd-O: 2.26, 2.36 Å; Cd-N: 2.48 Å); $Cd(his)_2H_2O$ 2.378 Å (Cd-O: 2.26 Å; Cd-N: 2.41-2.48 Å, Table S3 and Fig. 4). Hence, the small differences in Cd isotope fractionation between the two complexes might have been demonstrated by the

381 distinct coordination and bond lengths of the two complexes.

382

383 *3.4. Error analysis for Cd isotope fractionation*

384

385 Vacuo and solvation models can cause isotope fractionation factors inaccuracies
386 (Hill and Schauble, 2008; Yang et al., 2015). In ideal vacuum gaseous conditions, the
387 influence of the surrounding environment such as solvents on the solute molecules in
388 the real system is ignored. To overcome this limitation, some solvent models were
389 established to simulate the effects of solvents on solutes. The polarized continuum
390 models (PCMs) are widely used to simulate the aqueous environment (Tomasi et al.,
391 2005; Tsipis, 2014). However, Yang et al. (2015) found that the bond lengths
392 optimized by IEFPCM model are larger than those by vacuo model and the $10^3\ln(\beta_{114-110})$
393 results calculated in the IEFPCM model are smaller than those in vacuo model,
394 and thought that the optimized structures and lnβ values of Cd complexes calculated
395 in vacuo are more consistent with the experimental data. For comparison, the implicit
396 solvation models IEFPCM (the integral-equation-formalism versions of PCM) and
397 CPCM (conductor-like PCM) were used to calculate the optimized molecular
398 structures and $10^3\ln(\beta_{114-110})$ at 25℃ for studied complexes (Table S4 and S5), as well
399 as the model of $Cd(H_2O)_6^{2+}$ with second hydration sphere $Cd(H_2O)_{18}^{2+}$ (Table S6).
400 Our calculation showed that most of the bond lengths optimized in solution by this
401 study were larger than those in vacuum (Table S4). This was agreement with the
402 results of inorganic Cd complexes (Yang et al., 2015). For $10^3\ln(\beta_{114-110})$ values, not

only does difference exist between two implicit models and vacuum model but also between two implicit models. By comparing with vacuum model, IEFPCM and CPCM solvation models decrease the $10^3\ln\beta$ of $Cd(H_2O)_4^{2+}$ by 0.346 and 0.221 at 25℃ respectively, and increase the $10^3\ln\beta$ of $Cd(H_2O)_6^{2+}$ by 0.139 and 0.166 at 25℃ respectively. For $Cd(Hcit)(H_2cit)^-$, $CdH(cit)(H_2O)_4$, $Cd(cit)(H_2O)_3^-$ and $Cd(his)_2H_2O$, IEFPCM and CPCM model decrease the $10^3\ln\beta$ by 0.175-0.580 and 0.206-0.567 and increase the $10^3\ln\beta$ of $Cd(cys)(H_2O)_3^{2+}$ by 0.281 and 0.401 at 25℃ respectively. For $Cd(cit)_2^{4-}$, CdEDTA, $Cd(DMPS)_2^{4-}$, these two models increase the $10^3\ln\beta$ by less than 0.1 at 25℃. For $Cd(GS)_2(H_2O)_2^{2-}$, the IEFPCM solvation model decrease the $10^3\ln\beta$ by 0.109 and CPCM model increase the $10^3\ln\beta$ by less than 0.1 at 25℃, the implicit solvation models have different effects on Cd isotope fractionation (Table S5). The main reason may be that the simple harmonic vibrational frequencies have been polluted by translation and rotation which make the inaccurate for frequencies data in solvation models (Yang et al., 2015), and the levels of "pollution" may be different for different Cd complexes.

Setting the second hydration sphere is able to make the calculated frequencies closer to the experimental values and improve the $10^3\ln\beta$ for Ni and Zn (Fujii et al., 2014), the same phenomenon may occur in Cd hydrate species. Our calculation showed that for $Cd(H_2O)_6^{2+}$, the $10^3\ln\beta$ values for the explicit model as $Cd(H_2O)_{18}^{2+}$ is 2.377 and 1.990, 1.923 for explicit model + IEFPCM and explicit model + CPCM at 25℃ respectively. Compared with the vacuum model, the explicit model increases the $10^3\ln\beta$ values and explicit + implicit model decrease them (Table S6). The total

symmetric stretching mode of hexaaqua complexes, ν_1 CdO_6, is shown in Table S6. The calculated ν_1 frequency values of large cluster $Cd(H_2O)_{18}^{2+}$, $Cd(H_2O)_6^{2+}$ + IEFPCM and $Cd(H_2O)_6^{2+}$ + CPCM are closer to previous calculation and experimental data than that of $Cd(H_2O)_6^{2+}$ (Table S6), which means solvation models make the frequency values closer the literature values and the solvent effect on $10^3 ln\beta$ values are needed to be considered.

Frequency is another most frequently mentioned factor that may cause uncertainties or errors of the calculated reduced partition function ratios (Schauble et al., 2003, 2004; Schauble et al., 2007; Méheut et al., 2007, 2009; Weeks et al., 2007; Yang et al., 2015). For lack of experimental vibrational frequency of Cd organic complexes, it is impossible to evaluate the RPFR errors for them, and different vibration frequencies may lead to discrepant uncertainty in $10^3 ln(\beta_{114-110})$ values at 25□ (Vogt et al., 1993; Schauble, 2007; Yang et al., 2015). Based on existing experimental frequency data of $Cd(Hcit)(H_2cit)^-$ and this calculation, the maximum difference between them is 3.187%, and the average deviation is about 0.293%. Based on Schauble (2007, 2011), calculated frequencies may lead to an error of less than 0.6% for $10^3 ln(\beta_{114-110})$ values of $Cd(Hcit)(H_2cit)^-$.

3.5 Implications for Cd process tracing applications in biogeochemistry, supergene geochemistry and environmental science

Metal isotope fractionation can be used to trace processes that control the

447 distribution of an element in terrestrial and aquatic environments. Previous
448 experimental studies hypothesized that the Cd isotope fractionation is strongly linked
449 to Cd speciation to organic ligands with S donor atoms to detoxify and immobilize Cd
450 in living organisms (Horner et al., 2013; Wiggenhauser et al., 2016, 2021; Imseng et
451 al., 2019). Results by this study and Yang et al. (2015) revealed that an enrichment of
452 light isotopes occurs in thiol ligands when compared to hydrated Cd and Cd bound to
453 O/N donor atoms of organic ligands, which will strengthen not only Cd isotopes as a
454 process tracing tool, but also the understanding of Cd isotope cycling in aquatic and
455 terrestrial systems. For example, to reduce inputs of the toxic trace metal Cd into the
456 food chain of humans and animals, processes that control the mobility of Cd in
457 terrestrial and aquatic environments need to be well understood. The results that
458 heavy Cd isotopes preferably bind to oxygen and nitrogen donor atoms while light Cd
459 isotopes bind to sulfur donor atoms of organic ligands compared to hydrated Cd^{2+}
460 provides information on processes on the immobilization of Cd isotopes in living
461 organisms which are related to Cd detoxification processes with sulfur.

462 Furthermore, the strongest Cd isotope fractionation compared to hydrated Cd
463 occurred in chelating S donor ligands, particularly in a chelating S donor ligand in
464 which Cd is exclusively bound to S. Thus, our data confirms the hypothesis that the
465 retention of light isotopes in roots and shoots of grasses (Wiggenhauser et al., 2016,
466 2021; Imseng et al., 2019) and membranes of *E.Coli* (Horner et al., 2013) could be
467 induced by the immobilization of light Cd isotopes through strong Cd binding to
468 chelators with S donor atoms such as phytochelatins (Clemens et al. 2019). This

chelation would retain light Cd isotopes e.g., in the roots of cereals, while other chemical Cd species such as hydrated Cd that are enriched in heavy isotopes can be transported by membrane proteins towards the shoot. The Cd isotope fractionation induced by chelating thiols may have implications on Cd isotope fractionation in other plants than grasses. Cd hyperaccumulator plants can cope with high Cd concentrations and store, unlike cereals, the majority of the Cd taken up from soils in their shoots (Zhou et al. 2020). To cope with the high Cd shoot concentrations, Cd is mostly bound to O donor atoms of e.g., organic acids and to a lesser extent to S donors (Tian et al. 2011; Isaure et al. 2015). Based on our findings, the Cd isotope fractionation in Cd accumulating plants could potentially provide novel insights into the role of Cd binding to different donor atoms on the translocation of Cd within the shoot. Recent studies focused on Cd isotope fractionation in cacao since cacao beans often exceed the threshold values for Cd potentially leading to elevated Cd concentrations in chocolate (Moore et al. 2020; Barraza et al. 2019). Similar to grasses such as wheat, rice, and barley, cacao seems to retain Cd and its light isotopes in the roots (Moore et al. 2020). Our findings suggest that Cd binding to thiols may play also a crucial role to retain Cd in roots of cacao and thereby limit the Cd transport into cacao beans.

Our results further suggest that Cd ligands, especially thiols, may play a key role in Cd isotope fractionation in living organisms, soils, and waters. In this study, the Cd isotope fractionation between hydrated Cd and Cd chelated by S donor atoms was ~ 1‰. The largest Cd isotope fractionation that has been observed between roots and shoots of plants that strongly retain light Cd isotopes in roots was around 0.60 ‰

491 (Wiggenhauser et al. 2016, 2021; Imseng et al. 2018; Moore et al. 2020). The
492 difference between our results and the experimentally determined Cd isotopes
493 fractionation between root and shoots may be caused by additional isotope effects that
494 complement isotope effects at equilibrium. The transfer from root to shoot includes
495 membrane transport (Deng et al. 2019). This transport requires fast binding of Cd to a
496 metal binding site of a membrane protein prior to unidirectional membrane transport
497 (Wang et al., 2014; Zhao et al., 2016). Thus, membrane transport might be at least
498 partly kinetically controlled (Köbberich and Vance, 2017). Kinetically controlled
499 processes favor light isotopes through their faster reaction rates (Wiederhold, 2015)
500 while type of metal binding sites of a membrane transproters (e.g., cysteine, histidine)
501 might play an additional role for isotope fractionation during membrane transport.
502 Together, our results suggest that equilibrium Cd isotope fractionation in plants
503 induced by binding of Cd to organic molecules occur in parallel to kinetic isotope
504 effects.

505 In soils, sediments, and water, organic matter poses an important binding site for
506 Cd and partly controls the mobility of Cd. For instance, soil organic matter derives
507 from decomposed biomass and provides a mixture of O, N, and S donor atoms for Cd
508 in the solid and liquid phase of the soil (Karlsson et al., 2007; Tiberg et al., 2018).
509 Besides processes such as Cd sulfide precipitation and Cd uptake into phytoplankton,
510 soluble organic ligands might significantly control the Cd distribution in water
511 columns and sediments during the oceanic Cd cycle (Guinoiseau et al., 2018). Our
512 data implies that Cd sorption of Cd to organic matter can enrich or deplete the

hydrated Cd pool in heavy and could provide further insights into the role of specific binding sites of organic matter on Cd cycling in the environment.

4. Conclusion

This study provides a first prediction that describes Cd equilibrium isotope fractionation induced by Cd complexation to organic ligands. The $10^3 \ln\beta$ of $^{114}Cd/^{110}Cd$ for these investigated complexes decreased in the order of $Cd(Hcit)(H_2cit)^-$ > $Cd(cit)(H_2O)_3^-$ > $CdH(cit)(H_2O)_4$ > CdEDTA > $Cd(his)_2H_2O$ > $Cd(cit)_2^{4-}$ ≈ $Cd(H_2O)_6^{2+}$ > $Cd(H_2O)_4^{2+}$ > $Cd(cys)(H_2O)_3^{2+}$ > $Cd(GS)_2(H_2O)_2^{2-}$ > $Cd(DMPS)(H_2O)_2^-$ > $Cd(DMPS)_2^{4-}$ at 0 ~ 100℃. The sequence reveals that Cd complexation to organic ligands with O and N donor atoms are enriched in heavy isotopes while to organic ligands with S donor atoms are enriched with light isotopes. These results provide important information to advance Cd isotopes as a process tracing tool in complex biological systems and further improve the understanding of Cd isotope cycling in aquatic and terrestrial systems.

Acknowledgments

This research was supported financially by the National Natural Science Foundation of China (No. 41872160); the Key Project of National Natural Science Foundation of China (No. 41530315); the DREAM project of MOST of China (2016YFC0600401);

535 and the Swiss national research foundation (Early Postdoc.mobility, P2EZP2-
536 178618). We are also grateful for Professor Wang Zhixiang who provided us the
537 chance to conduct this study.

538

539 **Appendices. Supplementary material**

540

541 Table S1: Comparing the experimental vibrational frequencies with calculated results
542 (^{110}w) employed by four different exchange correlation functionals for
543 $Cd(Hcit)(H_2cit)^-$. Table S2: The fitting factors A, B for $10^3\ln(\beta_{114-110})=A\times10^6/T^2+B$ (T
544 is K). Table S3: The donor atoms, coordinated bond lengths (Å) and mean bond
545 lengths (Å) for Cd complexes. Table S4a: Optimized bond lengths (Å) of the Cd
546 hydration complexes and citrate complexes calculated with solvation models. Table
547 S4b: Optimized bond lengths (Å) of the organic Cd complexes calculated with
548 solvation models. Table S5: The $10^3\ln(\beta_{114-110})$ of Cd complexes calculated in vacuo
549 and solvation models (IEFPCM，CPCM) at 25°C. Table S6: The vibrational
550 frequencies (^{110}w) and $10^3\ln\beta$ values of $Cd(H_2O)_6^{2+}$ and $Cd(H_2O)_{18}^{2+}$.

551

552 **References**

553

554 Albarede, F., Télouk, P., Balter, V., Bondanese, V.P., Albalat, E., Oger, P.,
555 Bonaventura, P., Miossec, P., Fujii, T., 2016. Medical applications of Cu, Zn,
556 and S isotope effects. Metallomics 8, 1056–1070.

557 Albarède, F., Telouk, P., Lamboux, A., Jaouen, K., Balter, V., 2011. Isotopic evidence
558 of unaccounted for Fe and Cu erythropoietic pathways. Metallomics 3, 926–933.
559 Balter, V., Lamboux, A., Zazzo, A., Télouk, P., Leverrier, Y., Marvel, J., Moloney,
560 A.P., Monahan, F.J., Schmidt, O., Albarède, F., 2013. Contrasting Cu, Fe, and
561 Zn isotopic patterns in organs and body fluids of mice and sheep, with emphasis
562 on cellular fractionation. Metallomics 5, 1470–1482.
563 Becke, A.D., 1993a. Density- functional thermochemistry. III. The role of exact
564 exchange. J. Chem. Phys. 98, 5648–5652.
565 Becke, A.D., 1993b. A new mixing of Hartree–Fock and local density- functional
566 theories. J. Chem. Phys. 98, 1372–1377.
567 Bertoli, A.C., Carvalho, R., Freitas, M.P., Ramalho, T.C., Mancini, D.T., Oliveira,
568 M.C., de Varennes, A., Dias, A., 2015. Theoretical spectroscopic studies and
569 identification of metal-citrate (Cd and Pb) complexes by ESI-MS in aqueous
570 solution. Spectrochim. Acta Part A Mol. Biomol. Spectrosc. 137, 271–280.
571 Bigalke, M., Weyer, S., Wilcke, W., 2010. Copper isotope fractionation during
572 complexation with insolubilized humic acid. Environ. Sci. Technol. 44, 5496–
573 5502.
574 Bigeleisen, J., Mayer, M.G., 1947. Calculation of equilibrium constants for isotopic
575 exchange reactions. J. Chem. Phys. 15, 261–267.
576 Cao, Z.-Y., Sun, L.-H., Mou, R.-X., Zhou, R., Zhu, Z.-W., Chen, M.-X., 2014. A
577 novel method for the simultaneous analysis of seven biothiols in rice (Oryza
578 sativa L.) using hydrophilic interaction chromatography coupled with

electrospray tandem mass spectrometry. J. Chromatogr. B 976–977.

Cao, Z.-Z., Qin, M.-L., Lin, X.-Y., Zhu, Z.-W., Chen, M.-X., 2018. Sulfur supply reduces cadmium uptake and translocation in rice grains (Oryza sativa L.) by enhancing iron plaque formation, cadmium chelation and vacuolar sequestration. Environ. Pollut. 238, 76–84.

Carignan, J., Cardinal, D., Eisenhauer, A., Galy, A., Rehkämper, M., Wombacher, F., Vigier, N., 2004. A reflection on Mg, Cd, Ca, Li and Si isotopic measurements and related reference materials. Geostand. Geoanalytical Res. 28, 139–148.

Chrastný, V., Čadková, E., Vaněk, A., Teper, L., Cabala, J., Komárek, M., 2015. Cadmium isotope fractionation within the soil profile complicates source identification in relation to Pb–Zn mining and smelting processes. Chem. Geol. 405, 1–9.

Clark, T., Chandrasekhar, J., Spitznagel, G.W., Schleyer, P.V.R., 1983. Efficient diffuse function-augmented basis sets for anion calculations. III. The 3-21+G basis set for first-row elements, Li–F. J. Comput. Chem. 4, 294–301.

Clemens, S., 2019. Metal ligands in micronutrient acquisition and homeostasis. Plant. Cell Environ. 42, 2902–2912.

Clemens, S., Deinlein, U., Ahmadi, H., Höreth, S., Uraguchi, S., 2013. Nicotianamine is a major player in plant Zn homeostasis. BioMetals 26, 623–632.

Cloquet, C., Carignan, J., Libourel, G., Sterckeman, T., Perdrix, E., 2006. Tracing source pollution in soils using cadmium and lead isotopes. Environ. Sci. Technol. 40, 2525–2530.

601 Colaneri, M.J., Vitali, J., Kirschbaum, K., 2013. Electron paramagnetic resonance
602 spectroscopic study of copper hopping in doped bis(l-histidinato)cadmium
603 dihydrate. J. Phys. Chem. A 117, 3414–3427.
604 Deng, F., Yu, M., Martinoia, E., Song, W.-Y., 2019. Ideal Cereals With Lower
605 Arsenic and Cadmium by Accurately Enhancing Vacuolar Sequestration
606 Capacity. Front. Genet. 10, 322.
607 Dennington, R., Keith, T., Millam, J., 2009. GaussView, Version 5.0.8. Semichem
608 Inc.,Shawnee Mission, KS.
609 Delalande, O., Desvaux, H., Godat, E., Valleix, A., Junot, C., Labarre, J., Boulard, Y.,
610 2010. Cadmium – glutathione solution structures provide new insights into
611 heavy metal detoxification. FEBS J. 277, 5086–5096.
612 Francl, M.M., Pietro, W.J., Hehre, W.J., Binkley, J.S., Gordon, M.S., DeFrees, D.J.,
613 Pople, J.A., 1982. Self- consistent molecular orbital methods. XXIII. A
614 polarization- type basis set for second- row elements. J. Chem. Phys. 77, 3654–
615 3665.
616 Fransson, M. N., Barregard, L., Sällsten, G., Akerstrom, M., Johanson, G., 2014.
617 Physiologically-based toxicokinetic model for cadmium using markov-chain
618 monte carlo analysis of concentrations in blood, urine, and kidney cortex from
619 living kidney donors. Toxicol. Sci. 141, 365–376.
620 Frisch, M.J., Trucks, G.W., Schlegel, H.B., Scuseria, G.E., Robb, M.A., Cheeseman,
621 J.R., Scalmani, G., Barone, V., Mennucci, B., Petersson, G.A., Nakatsuji, H.,
622 Caricato, M., Li, X., Hratchian, H.P., Izmaylov, A.F., Bloino, J., Zheng, G.,

623 Sonnenberg, J.L., Hada, M., Ehara, M., Toyota, K., Fukuda, R., Hasegawa, J.,
624 Ishida, M., Nakajima, T., Honda, Y., Kitao, O., Nakai, H., Vreven, T.,
625 Montgomery Jr., J.A., Peralta, J.E., Ogliaro, F., Bearpark, M., Heyd, J.J.,
626 Brothers, E., Kudin, K.N., Staroverov, V.N., Kobayashi, R., Normand, J.,
627 Raghavachari, K., Rendell, A., Burant, J.C., Iyengar, S.S., Tomasi, J., Cossi, M.,
628 Rega, N., Millam, J. M., Klene, M., Knox, J.E., Cross, J.B., Bakken, V., Adamo,
629 C., Jaramillo, J., Gomperts, R., Stratmann, R.E., Yazyev, O., Austin, A.J.,
630 Cammi, R., Pomelli, C., Ochterski, J.W., Martin, R.L., Morokuma, K.,
631 Zakrzewski, V.G., Voth, G.A., Salvador, P., Dannenberg, J.J., Dapprich, S.,
632 Daniels, A.D., Farkas, Ö., Foresman, J.B., Ortiz, J.V., Cioslowski, J., Fox, D.J.,
633 2009. Gaussian 09, Revision A.01. Gaussian, Inc., Wallingford, CT

634 Fujii, T., Albarède, F., 2012. Ab initio calculation of the Zn isotope effect in
635 phosphates, citrates, and malates and applications to plants and soil. PLoS One 7,
636 e30726.

637 Fujii, T., Moynier, F., Blichert-Toft, J., Albarède, F., 2014. Density functional theory
638 estimation of isotope fractionation of Fe, Ni, Cu, and Zn among species relevant
639 to geochemical and biological environments. Geochim. Cosmochim. Acta 140,
640 553–576.

641 Fujii, T., Moynier, F., Pons, M.-L., Albarède, F., 2011. The origin of Zn isotope
642 fractionation in sulfides. Geochim. Cosmochim. Acta 75, 7632–7643.

643 Guinoiseau, D., Galer, S.J.G., Abouchami, W., 2018. Effect of cadmium sulphide
644 precipitation on the partitioning of Cd isotopes: Implications for the oceanic Cd

cycle. Earth Planet. Sci. Lett. 498, 300–308.

Gunawardana, B., Singhal, N., Johnson, A., 2010. Amendments and their combined application for enhanced copper, cadmium, lead uptake byLolium perenne. Plant Soil 329, 283–294.

Hay, P.J., Wadt, W.R., 1985. Ab initio effective core potentials for molecular calculations.Potentials for K to Au including the outer most core orbitals. J. Chem. Phys. 82, 299–310.

Hill, P.S., Schauble, E.A., 2008. Modeling the effects of bond environment on equilibrium iron isotope fractionation in ferric aquo-chloro complexes. Geochim. Cosmochim. Acta 72, 1939–1958.

Hoch, E., Lin, W., Chai, J., Hershfinkel, M., Fu, D., Sekler, I., 2012. Histidine pairing at the metal transport site of mammalian ZnT transporters controls Zn^{2+} over Cd^{2+} selectivity. Proc. Natl. Acad. Sci. 109, 7202–7207.

Hoefs, J., 2015. Isotope fractionation processes of selected elements BT - stable isotope geochemistry, in: Hoefs, J. (Ed.), . Springer International Publishing, Cham, pp. 47–190.

Horner, T.J., Lee, R.B.Y., Henderson, G.M., Rickaby, R.E.M., 2013. Nonspecific uptake and homeostasis drive the oceanic cadmium cycle. Proc. Natl. Acad. Sci. 110, 2500 – 2505.

Horner, T.J., Rickaby, R.E.M., Henderson, G.M., 2011. Isotopic fractionation of cadmium into calcite. Earth Planet. Sci. Lett. 312, 243–253.

Imseng, M., Wiggenhauser, M., Keller, A., Müller, M., Rehkämper, M., Murphy, K.,

667 Kreissig, K., Frossard, E., Wilcke, W., Bigalke, M., 2019. Towards an
668 understanding of the Cd isotope fractionation during transfer from the soil to the
669 cereal grain. Environ. Pollut. 244, 834–844.
670 Imseng, M., Wiggenhauser, M., Keller, A., Müller, M., Rehkämper, M., Murphy, K.,
671 Kreissig, K., Frossard, E., Wilcke, W., Bigalke, M., 2018. Fate of Cd in
672 agricultural soils: a stable isotope approach to anthropogenic impact, soil
673 formation, and soil-plant cycling. Environ. Sci. Technol. 52, 1919–1928.
674 Isaure, M.-P., Huguet, S., Meyer, C.-L., Castillo-Michel, H., Testemale, D., Vantelon,
675 D., Saumitou-Laprade, P., Verbruggen, N., Sarret, G., 2015. Evidence of various
676 mechanisms of Cd sequestration in the hyperaccumulator Arabidopsis halleri, the
677 non-accumulator Arabidopsis lyrata, and their progenies by combined
678 synchrotron-based techniques. J. Exp. Bot. 66, 3201–3214.
679 Jalilehvand, F., Leung, B.O., Mah, V., 2009. Cadmium(II) complex formation with
680 cysteine and penicillamine. Inorg. Chem. 48, 5758–5771.
681 John, S.G., Kunzmann, M., Townsend, E.J., Rosenberg, A.D., 2017. Zinc and
682 cadmium stable isotopes in the geological record: A case study from the post-
683 snowball Earth Nuccaleena cap dolostone. Palaeogeogr. Palaeoclimatol.
684 Palaeoecol. 466, 202–208.
685 Jouvin, D., Louvat, P., Juillot, F., Maréchal, C.N., Benedetti, M.F., 2009. Zinc
686 isotopic fractionation: why organic matters. Environ. Sci. Technol. 43, 5747–
687 5754.
688 Kabata-Pendias, A., 2011. Trace elements in soils and plants, 4. ed. ed. CRC Press,

Boca Raton, Fla.

Karak, T., Paul, R.K., Das, D.K., Boruah, R.K., 2016. Complexation of DTPA and EDTA with Cd^{2+}: stability constants and thermodynamic parameters at the soil-water interface. Environ. Monit. Assess. 188, 670.

Karlsson, T., Elgh-Dalgren, K., Björn, E., Skyllberg, U., 2007. Complexation of cadmium to sulfur and oxygen functional groups in an organic soil. Geochim. Cosmochim. Acta 71, 604–614.

Khan, M.A., Castro-Guerrero, N., Mendoza-Cozatl, D.G., 2014. Moving toward a precise nutrition: preferential loading of seeds with essential nutrients over non-essential toxic elements. Front. Plant Sci. 5, 51.

Köbberich, M., Vance, D., 2017. Kinetic control on Zn isotope signatures recorded in marine diatoms. Geochim. Cosmochim. Acta 210, 97–113.

Kovács, A., Nemcsok, D.S., Kocsis, T., 2010. Bonding interactions in EDTA complexes. J. Mol. Struct. THEOCHEM 950, 93–97.

Krishnan, R., Binkley, J.S., Seeger, R., Pople, J.A., 1980. Self- consistent molecular orbital methods. XX. A basis set for correlated wave functions. J. Chem. Phys. 72, 650–654.

Lambelet, M., Rehkämper, M., van de Flierdt, T., Xue, Z., Kreissig, K., Coles, B., Porcelli, D., Andersson, P., 2013. Isotopic analysis of Cd in the mixing zone of Siberian rivers with the Arctic Ocean—New constraints on marine Cd cycling and the isotope composition of riverine Cd. Earth Planet. Sci. Lett. 361, 64–73.

Larner, F., McLean, C., Halliday, A., Roberts, B., 2019. Copper isotope compositions

711 of superoxide dismutase and metallothionein from post-mortem human frontal
712 cortex. Inorganics 7, 86.
713 Le Croizier, G., Lacroix, C., Artigaud, S., Le Floch, S., Munaron, J.-M., Raffray, J.,
714 Penicaud, V., Rouget, M.-L., Laë, R., Tito De Morais, L., 2019. Metal
715 subcellular partitioning determines excretion pathways and sensitivity to
716 cadmium toxicity in two marine fish species. Chemosphere 217, 754–762.
717 Lee, C., Yang, W., Parr, R.G., 1988. Development of the Colle-Salvetti correlation-
718 energy formula into a functional of the electron density. Phys. Rev. B 37, 785–
719 789.
720 Leitenmaier, B., Witt, A., Witzke, A., Stemke, A., Meyer-Klaucke, W., Kroneck,
721 P.M.H., Küpper, H., 2011. Biochemical and biophysical characterisation yields
722 insights into the mechanism of a Cd/Zn transporting ATPase purified from the
723 hyperaccumulator plant Thlaspi caerulescens. Biochim. Biophys. Acta -
724 Biomembr. 1808, 2591–2599.
725 Li, D., Li, M.-L., Liu, W.-R., Qin, Z.-Z., Liu, S.-A., 2018. Cadmium isotope ratios of
726 standard solutions and geological reference materials measured by MC-ICP-MS.
727 Geostand. Geoanalytical Res. 42, 593–605.
728 Liu, Q., Tossell, J.A., Liu, Y., 2010. On the proper use of the Bigeleisen–Mayer
729 equation and corrections to it in the calculation of isotopic fractionation
730 equilibrium constants. Geochim. Cosmochim. Acta 74, 6965–6983.
731 Liu, Y., Xiao, T., Perkins, R.B., Zhu, J., Zhu, Z., Xiong, Y., Ning, Z., 2017. Geogenic
732 cadmium pollution and potential health risks, with emphasis on black shale. J.

733 Geochemical Explor. 176, 42–49.
734 Marentes, E., Rauser, W.E., 2007. Different proportions of cadmium occur as Cd-
735 binding phytochelatin complexes in plants. Physiol. Plant. 131, 291–301.
736 Maret, W., Moulis, J.-M., 2013. The bioinorganic chemistry of cadmium in the
737 context of its toxicity. Met. Ions Life Sci. 11, 1–29.
738 Marković, T., Manzoor, S., Humphreys-Williams, E., Kirk, G.J.D., Vilar, R., Weiss,
739 D.J., 2017. Experimental determination of zinc isotope fractionation in
740 complexes with the phytosiderophore 2′-deoxymugeneic acid (DMA) and its
741 structural analogues, and implications for plant uptake mechanisms. Environ. Sci.
742 Technol. 51, 98–107.
743 McLean, A.D., Chandler, G.S., 1980. Contracted Gaussian basis sets for molecular
744 calculations. I. Second row atoms, Z=11–18. J. Chem. Phys. 72, 5639–5648.
745 McLean, J.E., Pabst, M.W., Miller, C.D., Dimkpa, C.O., Anderson, A.J., 2013. Effect
746 of complexing ligands on the surface adsorption, internalization, and bioresponse
747 of copper and cadmium in a soil bacterium, Pseudomonas putida. Chemosphere
748 91, 374–382.
749 Méheut, M., Lazzeri, M., Balan, E., Mauri, F., 2007. Equilibrium isotopic
750 fractionation in the kaolinite, quartz, water system: Prediction from first-
751 principles density-functional theory. Geochim. Cosmochim. Acta 71, 3170–3181.
752 Méheut, M., Lazzeri, M., Balan, E., Mauri, F., 2009. Structural control over
753 equilibrium silicon and oxygen isotopic fractionation: A first-principles density-
754 functional theory study. Chem. Geol. 258, 28–37.

Moore, R.E.T., Ullah, I., de Oliveira, V.H., Hammond, S.J., Strekopytov, S., Tibbett, M., Dunwell, J.M., Rehkämper, M., 2020. Cadmium isotope fractionation reveals genetic variation in Cd uptake and translocation by Theobroma cacao and role of natural resistance-associated macrophage protein 5 and heavy metal ATPase-family transporters. Hortic. Res. 7, 71.

Morgan, J.L.L., Wasylenki, L.E., Nuester, J., Anbar, A.D., 2010. Fe Isotope fractionation during equilibration of Fe−organic complexes. Environ. Sci. Technol. 44, 6095–6101.

Moynier, F., Fujii, T., 2017. Theoretical isotopic fractionation of magnesium between chlorophylls. Sci. Rep. 7, 6973.

Moynier, F., Fujii, T., Shaw, A.S., Le Borgne, M., 2013. Heterogeneous distribution of natural zinc isotopes in mice. Metallomics 5, 693–699.

Pal, R., Kaur, R., Rajwar, D., Rai, J., 2019. Induction of non-protein thiols and phytochelatins by cadmium in Eichhornia crassipes. Int. J. Phytoremediation 21, 1–9.

Pallavicini, N., Engström, E., Baxter, D.C., Öhlander, B., Ingri, J., Rodushkin, I., 2014. Cadmium isotope ratio measurements in environmental matrices by MC-ICP-MS. J. Anal. At. Spectrom. 29, 1570–1584.

Panfili, F., Schneider, A., Vives, A., Perrot, F., Hubert, P., Pellerin, S., 2009. Cadmium uptake by durum wheat in presence of citrate. Plant Soil 316, 299–309.

Prévéral, S., Gayet, L., Moldes, C., Hoffmann, J., Mounicou, S., Gruet, A., Reynaud, F., Lobinski, R., Verbavatz, J.-M., Vavasseur, A., Forestier C., 2009. A common

777 highly conserved cadmium detoxification mechanism from bacteria to humans:
778 heavy metal tolerance conferred by the atp-binding cassette (abc) transporter
779 sphmt1 requires glutathione but not metal-chelating phytochelatin peptides. J.
780 Biol. Chem. 284, 4936–4943.
781 Puschenreiter, M., Gruber, B., Wenzel, W.W., Schindlegger, Y., Hann, S., Spangl, B.,
782 Schenkeveld, W.D.C., Kraemer, S.M., Oburger, E., 2017. Phytosiderophore-
783 induced mobilization and uptake of Cd, Cu, Fe, Ni, Pb and Zn by wheat plants
784 grown on metal-enriched soils. Environ. Exp. Bot. 138, 67–76.
785 Ramalho, T.C., Figueroa-Villar, J.D., 2002. Thermodynamic evaluation of complexes
786 of zinc and cadmium that mimetize metallic centers in transcription factors. J.
787 Mol. Struct. THEOCHEM 580, 217–223.
788 Rehkämper, M., Wombacher, F., Horner, T.J., Xue, Z., 2011. Natural and
789 anthropogenic Cd isotope variations. Handbook of Environmental Isotope
790 Geochemistry. Springer, Berlin Heidelberg, pp. 125–154.
791 Richet, P., Bottinga, Y., Javoy, M., 1977. A Review of hydrogen, carbon, nitrogen,
792 oxygen, sulphur, and chlorine stable isotope fractionation among gaseous
793 molecules. Annu. Rev. Earth Planet. Sci. 5, 65–110.
794 Ryan, B.M., Kirby, J.K., Degryse, F., Scheiderich, K., McLaughlin, M.J., 2014.
795 Copper isotope fractionation during equilibration with natural and synthetic
796 ligands. Environ. Sci. Technol. 48, 8620–8626.
797 Salmanzadeh, M., Hartland, A., Stirling, C.H., Balks, M.R., Schipper, L.A., Joshi, C.,
798 George, E., 2017. Isotope tracing of long-term cadmium fluxes in an agricultural

soil. Environ. Sci. Technol. 51, 7369–7377.

Satarug, S., Garrett, S.H., Sens, M.A., Sens, D.A., 2010. Cadmium, environmental exposure, and health outcomes. Environ. Health Perspect. 118, 182–190.

Schauble, E., Rossman, G.R., Taylor, H.P., 2004. Theoretical estimates of equilibrium chromium-isotope fractionations. Chem. Geol. 205, 99–114.

Schauble, E.A., 2007. Role of nuclear volume in driving equilibrium stable isotope fractionation of mercury, thallium, and other very heavy elements. Geochim. Cosmochim. Acta 71, 2170–2189.

Schauble, E. A., 2011. First-principles estimates of equilibrium magnesium isotope fractionation in silicate, oxide, carbonate and hexaaquamagnesium(2+) crystals. Geochim. Cosmochim. Acta 75(3), 844-869.

Schauble, E. A., Rossman, G.R., Taylor, H.P., 2003. Theoretical estimates of equilibrium chlorine-isotope fractionations. Geochim. Cosmochim. Acta 67, 3267–3281.

Seth, C., Remans, T., Keunen, E., Jozefczak, M., Gielen, H., Opdenakker, K., Weyens, N., Vangronsveld, J., Cuypers, A., 2011. Phytoextraction of toxic metals: A central role for glutathione. Plant. Cell Environ. 35, 334–346.

Sieber, M., Conway, T.M., de Souza, G.F., Obata, H., Takano, S., Sohrin, Y., Vance, D., 2019. Physical and biogeochemical controls on the distribution of dissolved cadmium and its isotopes in the Southwest Pacific Ocean. Chem. Geol. 511, 494–509.

Sigel, A., Sigel, H., Sigel, R.K. (Eds.), 2013. Cadmium: from toxicity to essentiality,

metal ions in life sciences. Springer Netherlands, Dordrecht.

Siddiqui, K.A., Mehrotra, G.K., Narvi, S.S., Butcher, R.J., 2011. Molecular self-assembly of cadmium-triazolate complexes via hydrogen bonding: Synthesis, structures and photoluminescent properties. Inorg. Chem. Commun. 14, 814–817.

Smith, A., Barupala, D., Stemmler, T., Rosenzweig, A., 2015. A new metal binding domain involved in cadmium, cobalt and zinc transport. Nat. Chem. Biol. 11.

Sóvágó, I., Várnagy, K., 2013. Cadmium(II) complexes of amino acids and peptides BT - Cadmium: from toxicity to essentiality, in: Sigel, A., Sigel, H., Sigel, R.K.O. (Eds.), . Springer Netherlands, Dordrecht, pp. 275–302.

Spitznagel, G.W., Clark, T., von Ragué Schleyer, P., Hehre, W.J., 1987. An evaluation of the performance of diffuse function-augmented basis sets for second row elements, Na-Cl. J. Comput. Chem. 8, 1109–1116.

Thévenod, F., Fels, J., Lee, W.-K., Zarbock, R., 2019. Channels, transporters and receptors for cadmium and cadmium complexes in eukaryotic cells: myths and facts. BioMetals 32, 469–489.

Tian, S., Lu, L., Labavitch, J., Yang, X., He, Z., Hu, H., Sarangi, R., Newville, M., Commisso, J., Brown, P., 2011. Cellular Sequestration of Cadmium in the Hyperaccumulator Plant Species Sedum alfredii. Plant Physiol. 157, 1914–1925.

Tiberg, C., Sjöstedt, C., Gustafsson, J.P., 2018. Metal sorption to Spodosol Bs horizons: Organic matter complexes predominate. Chemosphere 196, 556–565.

Tomasi, J., Mennucci, B., Cammi, R., 2005. Quantum mechanical continuum solvation models. Chem. Rev. 105, 2999–3094.

Tsipis, A.C., 2014. DFT flavor of coordination chemistry. Coord. Chem. Rev. 272, 1–29.

Urey, H.C., 1947. The thermodynamic properties of isotopic substances. J. Chem. Soc. 562–581.

Vogt, N., Haaland, A., Martinsen, K.-G., Vogt, J., Grenthe, I., Li, K., MIlanova, R., Nakata, H., Nasiri, A., Tsuda, T., 1993. Molecular parameters of gaseous CdCl2 from electron diffraction and vibrational Spectroscopic data. Acta Chem. Scand. 47, 937–939.

Wang, K. T., Sitsel, O., Meloni, G., Autzen, H., Andersson, M., Klymchuk, T., Nielsen, A., Rees, D., Nissen, P., Gourdon, P., 2014. Structure and mechanism of Zn^{2+}-transporting P-type ATPases. Nature 514.

Wang, M.-J., Wang, W.-X., 2009. Cadmium in three marine phytoplankton: Accumulation, subcellular fate and thiol induction. Aquat. Toxicol. 95, 99–107.

Wasylenki, L.E., Swihart, J.W., Romaniello, S.J., 2014. Cadmium isotope fractionation during adsorption to Mn oxyhydroxide at low and high ionic strength. Geochim. Cosmochim. Acta 140, 212–226.

Weeks, C.L., Anbar, A.D., Wasylenki, L.E., Spiro, T.G., 2007. Density functional theory analysis of molybdenum isotope fractionation. J. Phys. Chem. A 111, 12434–12438.

Wei, R., Guo, Q., Wen, H., Liu, C., Yang, J., Peters, M., Hu, J., Zhu, G., Zhang, H., Tian, L., Han, X., Ma, J., Zhu, C., Wan, Y., 2016. Fractionation of stable cadmium isotopes in the cadmium tolerant ricinus communis and

865 hyperaccumulator solanum nigrum. Sci. Rep. 6, 24309.
866 Wiederhold, J.G., 2015. Metal stable isotope signatures as tracers in environmental
867 geochemistry. Environ. Sci. Technol. 49, 2606–2624.
868 Wierzbicka, M.H., Przedpełska, E., Ruzik, R., Ouerdane, L., Połeć-Pawlak, K., Jarosz,
869 M., Szpunar, J., Szakiel, A., 2007. Comparison of the toxicity and distribution of
870 cadmium and lead in plant cells. Protoplasma 231, 99.
871 Wiggenhauser, M., Aucour, A.-M., Bureau, S., Campillo, S., Telouk, P., Romani, M.,
872 Ma, J.F., Landrot, G., Sarret, G., 2021. Cadmium transfer in contaminated soil-
873 rice systems: Insights from solid-state speciation analysis and stable isotope
874 fractionation. Environ. Pollut. 269, 115934.
875 Wiggenhauser, M., Bigalke, M., Imseng, M., Müller, M., Keller, A., Murphy, K.,
876 Kreissig, K., Rehkämper, M., Wilcke, W., Frossard, E., 2016. Cadmium isotope
877 fractionation in soil–wheat systems. Environ. Sci. Technol. 50, 9223–9231.
878 Wiggenhauser, M., Bigalke, M., Imseng, M., Keller, A., Archer, C., Wilcke,
879 W.,Frossard, E., 2018. Zinc isotope fractionation during grain filling of wheat
880 and a comparison of zinc and cadmium isotope ratios in identical soil–plant
881 systems. New Phytol. 219, 195–205.
882 Wombacher, F., Rehkämper, M., 2004. Problems and suggestions concerning the
883 notation of cadmium stable isotope compositions and the use of reference
884 materials. Geostand. Geoanalytical Res. 28, 173–178.
885 Wu, Z., Zhang, C., Yan, J., Ge, Y., 2013. Separation and quantification of cysteine,
886 glutathione and phytochelatins in rice (Oryza sativa L.) upon cadmium exposure

using reverse phase ultra performance liquid chromatography (RP-UPLC) with fluorescence detection. Anal. Methods 5, 6147–6152.

Yang, J., Li, Y., Liu, S., Tian, H., Chen, C., Liu, J., Shi, Y., 2015. Theoretical calculations of Cd isotope fractionation in hydrothermal fluids. Chem. Geol. 391, 74–82.

Yang, W.-J., Ding, K.-B., Zhang, P., Qiu, H., Cloquet, C., Wen, H.-J., Morel, J.-L., Qiu, R.-L., Tang, Y.-T., 2019. Cadmium stable isotope variation in a mountain area impacted by acid mine drainage. Sci. Total Environ. 646, 696–703.

Zeini Jahromi, E., Gailer, J., Pickering, I.J., George, G.N., 2014. Structural characterization of Cd^{2+} complexes in solution with DMSA and DMPS. J. Inorg. Biochem. 136, 99–106.

Zelano, I.O., Cloquet, C., Fraysse, F., Dong, S., Janot, N., Echevarria, G., Montargès-Pelletier, E., 2018. The influence of organic complexation on Ni isotopic fractionation and Ni recycling in the upper soil layers. Chem. Geol. 483, 47–55.

Zhang, S.-N., Gu, Y., Zhu, Z.-L., Hu, S.-H., Kopittke, P.M., Zhao, F.-J., Wang, P., 2021. Stable isotope fractionation of cadmium in the soil-rice-human continuum. Sci. Total Environ. 761, 143262.

Zhang, Y., Wen, H., Zhu, C., Fan, H., Cloquet, C., 2018. Cadmium isotopic evidence for the evolution of marine primary productivity and the biological extinction event during the Permian-Triassic crisis from the Meishan section, South China. Chem. Geol. 481, 110–118.

Zhang, Y., Wen, H., Zhu, C., Fan, H., Luo, C., Liu, J., Cloquet, C., 2016. Cd isotope

fractionation during simulated and natural weathering. Environ. Pollut. 216, 9–17.

Zhao, C.-M., Campbell, P., Wilkinson, K., 2016. When are metal complexes bioavailable? Environ. Chem. 13, 425–433.

Zhou, J.-W., Li, Z., Liu, M.-S., Yu, H.-M., Wu, L.-H., Huang, F., Luo, Y.-M., Christie, P., 2020. Cadmium Isotopic Fractionation in the Soil–Plant System during Repeated Phytoextraction with a Cadmium Hyperaccumulating Plant Species. Environ. Sci. Technol. 54, 13598–13609.

Zhu, C., Wen, H., Zhang, Y., Fan, H., Fu, S., Xu, J., Qin, T., 2013. Characteristics of Cd isotopic compositions and their genetic significance in the lead–zinc deposits of SW China. Sci. China Earth Sci. 56 (12), 2056–2065.

Zhu, C., Wen, H., Zhang, Y., Fan, H., 2016. Cadmium and sulfur isotopic compositions of the Tianbaoshan Zn–Pb–Cd deposit, Sichuan Province, China. Ore Geol. Rev. 76, 152–162.

Zhu, C., Wen, H., Zhang, Y., Yin, R., Cloquet, C., 2018. Cd isotope fractionation during sulfide mineral weathering in the Fule Zn-Pb-Cd deposit, Yunnan Province, Southwest China. Science of The Total Environment. 616-617, 64-72.

Zorrig, W., Rouached, A., Shahzad, Z., Abdelly, C., Davidian, J.-C., Berthomieu, P., 2010. Identification of three relationships linking cadmium accumulation to cadmium tolerance and zinc and citrate accumulation in lettuce. J. Plant Physiol. 167, 1239–1247.

930 **Figure Captions:**

931

932 **Fig. 1.** Optimized molecular structures for various Cd species. a-b: Cd hydrate; c-f: Cd-citrate, the
933 original source of the structure derives from Bertoli et al. (2015) and Fujii et al. (2012); g:
934 CdEDTA (Kovács et al., 2010); h: Cd-histidine (Colaneri et al., 2013); i-j: Cd-DMPS (Zeini
935 Jahromi et al., 2014); k: Cd-cysteine (Jalilehvand et al., 2009 and Fujii et al., 2014); l: Cd-
936 glutathione (Delalande et al., 2010). Abbreviations are cit (citrate), EDTA
937 (ethylenediaminetetraacetic acid), his (histidine), DMPS (dimercaptopropane sulfonic acid), cys
938 (cysteine), and deprotonated glutathione (GSH) is shown as GS. Symbol keys: H (white), C
939 (grey), N (blue), O (red), S (purple), Cd (yellow).

940 **Fig. 2.** Temperature dependence of $10^3\ln(\beta_{114-110})$ for Cd hydrate, citrate, EDTA, histidine, DMPS,
941 cysteine and glutathione complexes. X-axis shows the function of $10^6/T^2$ (lower shaft) and
942 corresponding temperature (upper shaft, 0-100□), Y-axis shows the $10^3\ln(\beta_{114-110})$ values.

943 **Fig. 3.** Cd ($^{114}Cd/^{110}Cd$) isotopic variations with different donor atoms at 25℃. The complexes
944 with O donor atoms are shown as ⍰; N,O donor complexes as Δ; S,O donor complexes as □; S
945 donor complexes as ○. For O donor complexes, the order of $10^3\ln(\beta_{114-110})$ values at 25℃ from
946 small to large is $Cd(H_2O)_4^{2+}$ < $Cd(H_2O)_6^{2+}$ ≈ $Cd(cit)_2^{4-}$ < $CdH(cit)(H_2O)_4$ < $Cd(cit)(H_2O)_3^-$ <
947 $Cd(Hcit)(H_2cit)^-$; For N,O donor complexes, the order is $Cd(his)_2H_2O$ < CdEDTA; For S,O donor
948 complexes, the order is $Cd(DMPS)(H_2O)_2^-$ < $Cd(GS)_2(H_2O)_2^{2-}$ < $Cd(cys)(H_2O)_3^{2+}$; The S donor
949 complex is $Cd(DMPS)_2^{4-}$.

950 **Fig. 4.** Reduced partition function ratios, $10^3\ln(\beta_{114-110})$ vs. mean bond length (Å) at 25℃. Just as
951 Fig. 3, the complexes with O donor atoms are shown as ⍰, including $Cd(H_2O)_4^{2+}$, $Cd(H_2O)_6^{2+}$,

952 $Cd(cit)_2^{4-}$, $Cd(Hcit)(H_2cit)^-$, $CdH(cit)(H_2O)_4$ and $Cd(cit)(H_2O)_3^-$; N,O donor complexes as Δ,

953 including CdEDTA and $Cd(his)_2H_2O$; S,O donor complexes as □, including $Cd(DMPS)(H_2O)_2^-$,

954 $Cd(cys)(H_2O)_3^{2+}$ and $Cd(GS)_2(H_2O)_2^{2-}$; S donor complex as ○, is $Cd(DMPS)_2^{4-}$.

955

Figure

Click here to access/download;Figure;FIG1.tif

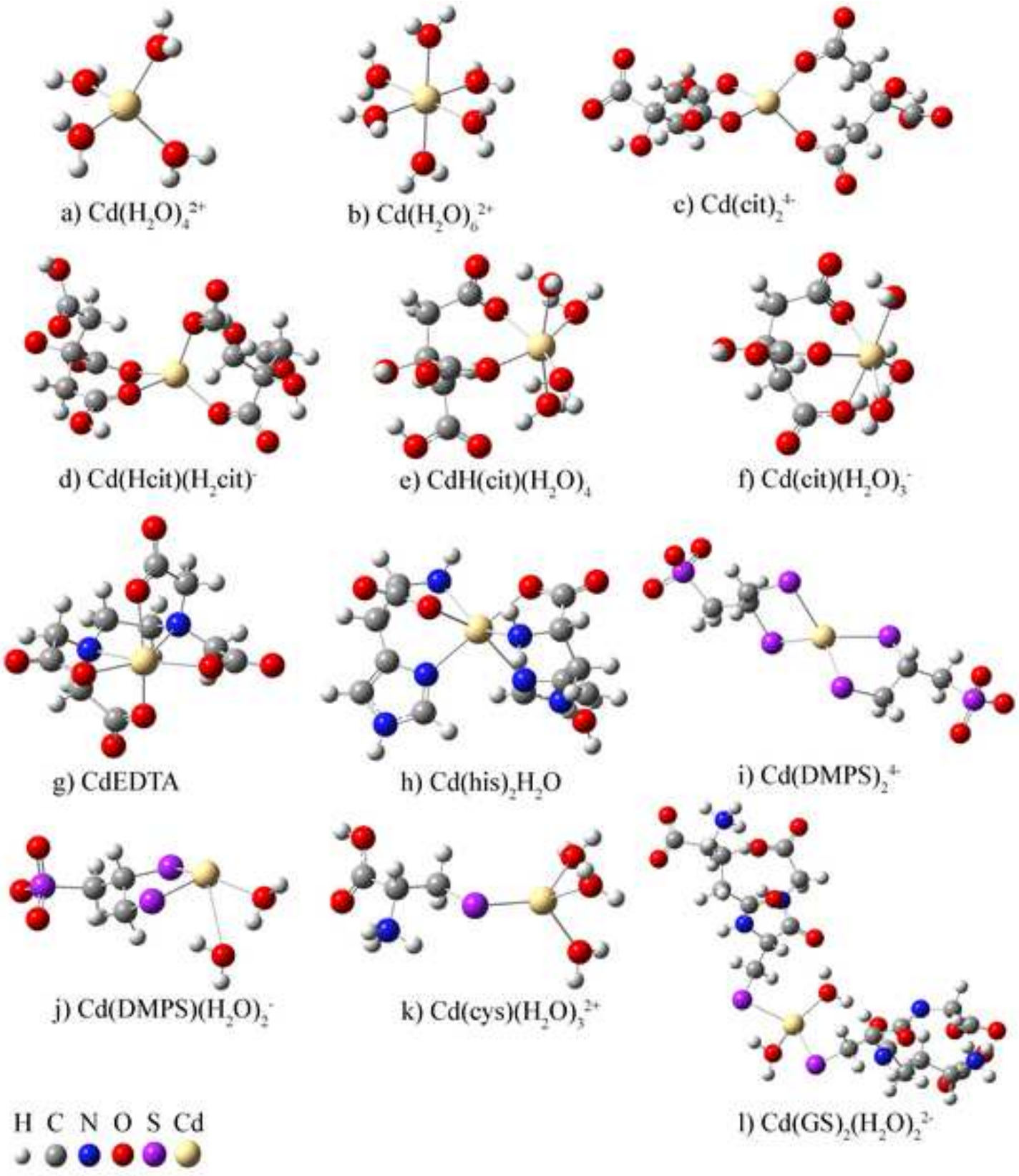

Figure

Click here to access/download;Figure;FIG2.tif

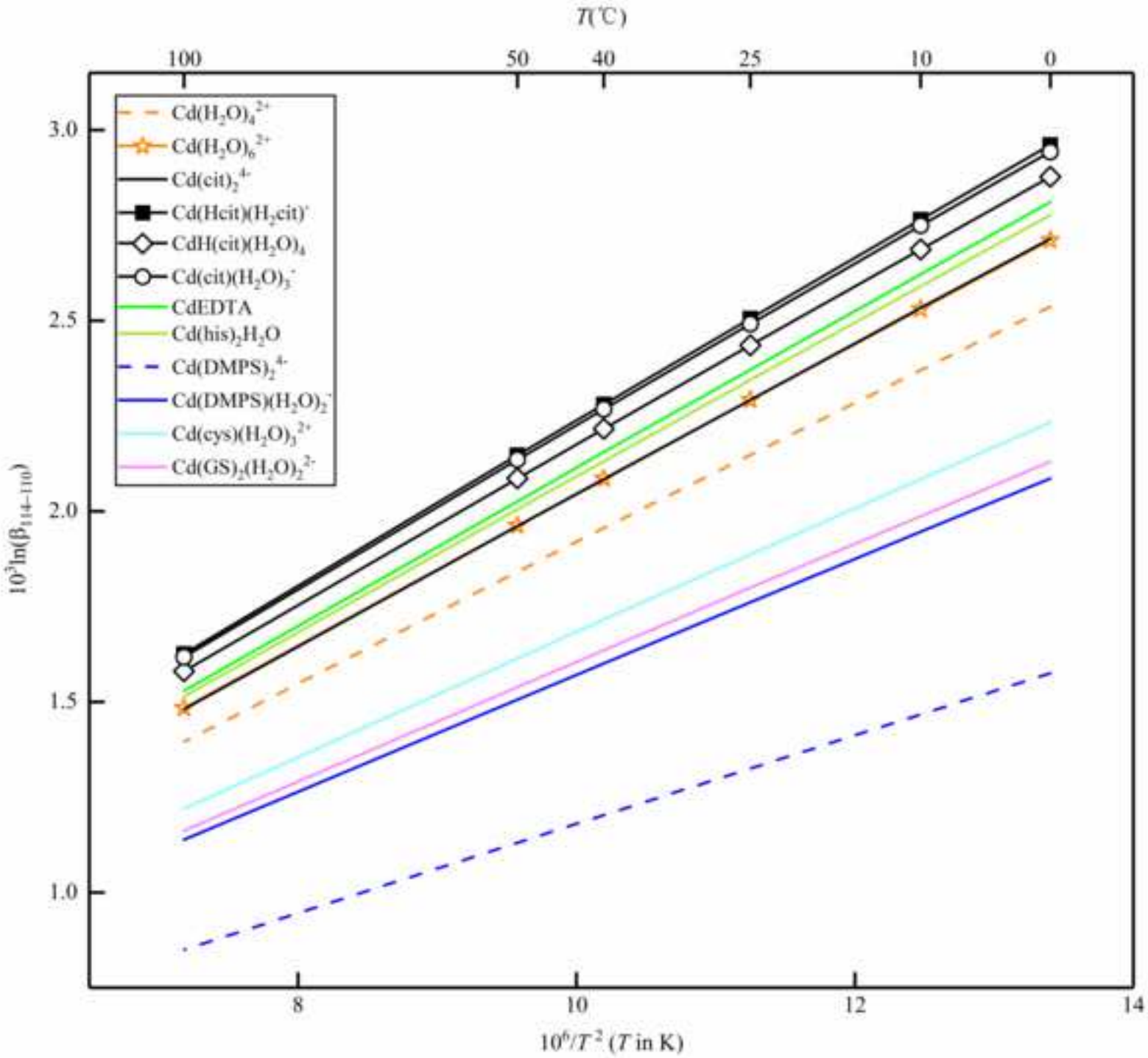

Figure

Click here to access/download;Figure;FIG3.tif

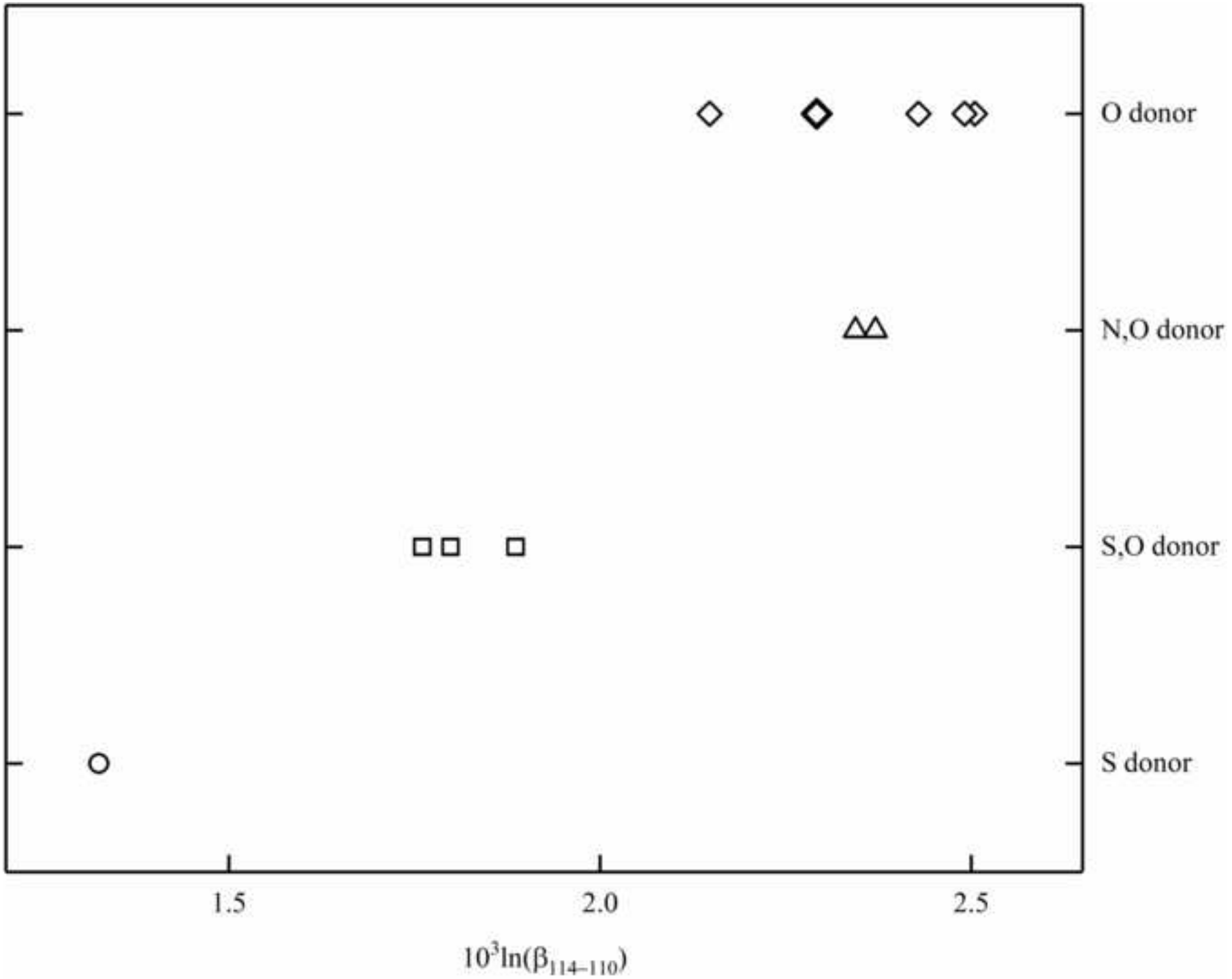

Figure

Click here to access/download;Figure;FIG4.tif

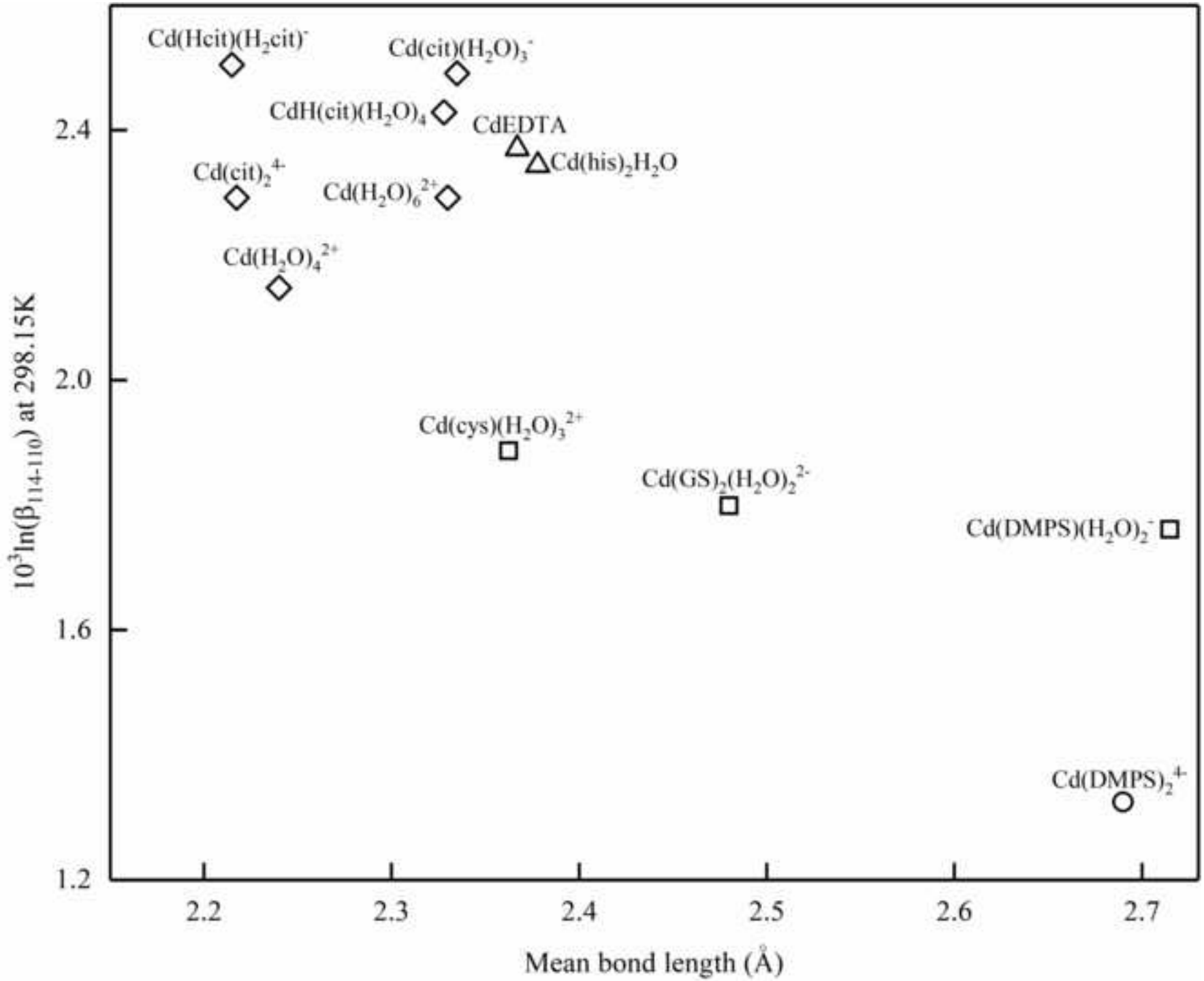

Table 1a Optimized bond lengths (Å) of the Cd hydration complexes and citrate complexes.

	$Cd(H_2O)_4^{2+}$	$Cd(H_2O)_6^{2+}$	$Cd(cit)_2^{4-}$	$Cd(Hcit)(H_2cit)^-$	$CdH(cit)(H_2O)_4$	$Cd(cit)(H_2O)_3^-$
Cd-O	2.24	2.33	2.22,2.21	2.20,2.14, 2.14,2.38	2.24,2.31,2.31, 2.37,2.34,2.40	2.24,2.28,2.29, 2.43,2.42,2.35
	2.24[a]	2.33 [a]	2.34-2.37[b]			

[a] Yang et al., 2015

[b] Bertoli et al., 2015

Table 1b Optimized bond lengths (Å) of the organic Cd complexes.

	CdEDTA	$Cd(his)_2H_2O$	$Cd(DMPS)_2^{4-}$	$Cd(DMPS)(H_2O)_2^-$	$Cd(cys)(H_2O)_3^{2+}$	$Cd(GS)_2(H_2O)_2^{2-}$
Cd-O	2.26,2.36	2.26		2.39,3.51	2.33,2.32,2.32	2.29,2.54
	2.24,2.40[a]	2.48[b]		2.39[c]		
Cd-N	2.48	2.41,2.45, 2.41,2.48				
	2.46[a]	2.287,2.29[b]				
Cd-S			2.70,2.68, 2.67,2.71	2.51,2.45	2.48	2.51,2.58
			2.57[c]	2.48[c]	2.52-2.54[d]	2.53-2.55[e]

[a] Kovács et al., 2010

[b] Colaneri et al., 2013

[c] Zeini Jahromi et al., 2014

[d] Jalilehvand et al., 2009

[e] Isaure et al., 2015

Table 2 Comparing the experimental vibrational frequencies with calculated results for $Cd(Hcit)(H_2cit)^-$.

w/cm^{-1}	Vibration Modes	$Cd(Hcit)(H_2cit)^-$			
		EXP[a]	^{114}w	^{110}w	$10^3(1-^{114}w/^{110}w)$
w_1	$\tau(HCH) + \nu(CO)$	1027.05	1041.1681	1041.1686	0.0005
w_2	$\rho(HCH) + \nu(CC)$	1078.98	1079.978	1079.9783	0.0003
w_3	$\tau(HCH) + \nu(CC)$	1095.98	1084.5717	1084.5721	0.0004
w_4	$\delta_{sciss}(HCH)$	1207.78	1201.8587	1201.8594	0.0006
w_5	$\rho(HCH) + \nu(CC) + \nu(CO)$	1248.26	1256.977	1256.9772	0.0002
w_6	$\omega(HCH) + \delta(OH)$	1280.53	1282.3539	1282.3541	0.0002
w_7	ν_s	1391.44	1387.1308	1387.1311	0.0002
w_8	$\nu_s(COO^-)$	1445.87	1444.8795	1444.8795	0.0000
w_9	$\nu_{as}(COO^-)$	1638.70	1690.9311	1690.9322	0.0007
w_{10}	$\nu(OH)$	3350.46	3328.6313	3328.6316	0.0001

δ: scissoring vibration; ρ: rocking vibration; ω: wagging vibration; τ: twisting vibration; ν_s: symmetrical stretching vibration; ν_{as}: asymmetrical stretching vibration.

[a] Experimental data obtained for Cd (not Cd isotope specific) by Bertoli et al. (2015).

Table 3 Calculated $10^3\ln(\beta_{114-110})$ for Cd complexes from 0 to 100 °C.

T(℃)	0	10	25	40	50	100
$Cd(H_2O)_4^{2+}$	2.537	2.370	2.148±0.0046	1.956	1.841	1.395
$Cd(H_2O)_6^{2+}$	2.711	2.530	2.292±0.0039	2.085	1.962	1.484
$Cd(cit)_2^{4-}$	2.715	2.533	2.292±0.0029	2.084	1.961	1.481
$Cd(Hcit)(H_2cit)^-$	2.961	2.765	2.505±0.0039	2.280	2.147	1.626
$CdH(cit)(H_2O)_4$	2.871	2.681	2.429±0.0038	2.211	2.081	1.576
$Cd(cit)(H_2O)_3^-$	2.943	2.749	2.491±0.0046	2.268	2.135	1.618
CdEDTA	2.811	2.621	2.371±0.0026	2.155	2.026	1.529
$Cd(his)_2H_2O$	2.777	2.590	2.344±0.0027	2.131	2.005	1.514
$Cd(DMPS)_2^{4-}$	1.575	1.467	1.325±0.0011	1.203	1.130	0.850
$Cd(DMPS)(H_2O)_2^-$	2.086	1.946	1.761±0.0022	1.601	1.506	1.138
$Cd(cys)(H_2O)_3^{2+}$	2.233	2.084	1.887±0.0026	1.716	1.614	1.220
$Cd(GS)_2(H_2O)_2^{2-}$	2.130	1.987	1.799±0.0025	1.635	1.539	1.162

Highlights:

- The isotope fractionation order of selected Cd organic complexes was given.
- Compared to hydrated Cd, organic complexes with O and N donors enrich heavier Cd isotopes, complexes with S donors enrich lighter isotopes.
- Organic ligands with S donors: chelating ligands were enriched in light isotope compared to non-chelating ligands.
- $Cd(H_2O)_6^{2+}$ is enriched in heavy isotope compared to $Cd(H_2O)_4^{2+}$.